Modeling contact between plastically deformable crystals at the micrometer scale

Ng Wei Siang, Kelvin

DOI
10.4233/uuid:74f87b87-6f01-4ce8-a22b-13a0dea41422

Publication date
2016

Document Version
Final published version

Citation (APA)
Ng Wei Siang, K. (2016). *Modeling contact between plastically deformable crystals at the micrometer scale*. [Dissertation (TU Delft), Delft University of Technology]. https://doi.org/10.4233/uuid:74f87b87-6f01-4ce8-a22b-13a0dea41422

Important note
To cite this publication, please use the final published version (if applicable).
Please check the document version above.

Modeling Contact between Plastically Deformable Crystals at the Micrometer Scale

MODELING CONTACT BETWEEN PLASTICALLY DEFORMABLE CRYSTALS AT THE MICROMETER SCALE

Proefschrift

ter verkrijging van de graad van doctor
aan de Technische Universiteit Delft,
op gezag van de Rector Magnificus prof. ir. K.C.A.M. Luyben,
voorzitter van het College voor Promoties,
in het openbaar te verdedigen op
donderdag 7 Juli 2016 om 12:30 uur

door

Kelvin NG WEI SIANG

Bachelor of Engineering (Aerospace Engineering),
Nanyang Technological University, Singapore,
geboren te Singapore, Singapore.

Dit proefschrift is goedgekeurd door de

promotor: Prof. dr. B. J. Thijsse
copromotor: Dr. L. Nicola

Samenstelling promotiecommissie:

Rector Magnificus,	voorzitter
Prof. dr. B. J. Thijsse,	Technische Universiteit Delft
Dr. L. Nicola,	Technische Universiteit Delft
Onafhankelijke leden:	
Prof. dr. J. Sietsma,	Technische Universiteit Delft
Prof. dr. ir. T. J. H. Vlugt,	Technische Universiteit Delft
Prof. dr. ir. A. S. J. Suiker,	Technische Universiteit Eindhoven
Dr. M. P. Ariza,	Universidad de Sevilla, Spanje
Dr. ir. M. van Drogen,	DAF Trucks N.V.

Keywords: Two Body Contact, Size Effect, Equivalent System, Static Friction, Friction Coefficient, Discrete Dislocation Plasticity

Printed by: Ipskamp drukkers

Cover Design: Kelvin Ng Wei Siang

ISBN 978-94-6186-686-8

An electronic version of this dissertation is available at
http://repository.tudelft.nl/.

To my mother, for always being there for me

CONTENTS

SUMMARY

The work presented in this thesis aims to gain a better understanding of the mechanical behavior of two metal bodies in contact that can both deform by dislocation plasticity. The analysis extends from previous contact studies that treated only a single plastically deformable body in contact with a rigid platen. Here, contact between a body with a sinusoidal surface having micrometer scale wavelength, a scale at which plasticity is known to be size dependent, and a platen is considered.

Simulations are performed using discrete dislocation plasticity, a method capable of describing micro-scale plasticity accurately, and predicting size effects. Plasticity is described as the collective motion of discrete dislocations, the fundamental carriers of plasticity. The dislocations are modeled as line singularities in an otherwise isotropic linear elastic medium. By that, the model contains the characteristic length scale of plasticity, the Burgers vector, which allows the model to capture plasticity size effects.

The novel formulation is described in Chapter 2. Contact between the bodies containing edge dislocations is treated as a constrained problem, and the solution for the image fields is obtained by minimizing the potential energy of both crystals while satisfying the contact constraints at the interface.

Despite the model is general, we focus first on contact between a plastically deformable body with a sinusoidal surface and a rigid or an elastic platen in Chapter 3. The difference with previous discrete dislocation plasticity contact studies is that before the effect of the rigid platen is prescribed by a set of boundary conditions, whereas both bodies in contact are explicitly modeled in this work. Two limit conditions, i.e. frictionless and full stick, are considered. Contrary to the result from previous studies we find that the true contact area, hence the true contact pressure are strongly affected by the contact conditions. However, the apparent contact area, apparent contact pressure and plastic deformation in the crystal are found to be unaffected. The exact morphology of the true contact area affects the local pressure but not its mean, or the overall plastic behavior.

In the same chapter, a size dependent plastic response is demonstrated, with smaller asperities being harder to deform than larger asperities. This is in agreement with previous discrete dislocation plasticity studies of contact. As expected,

the size effect is found to be less pronounced when the compliance of the platen is increased.

The analysis is then extended in Chapter 4 to a contact problem of two bodies that can both deform by discrete dislocation plasticity. We find that when both bodies in contact deform plastically, the plastic response is also size dependent. Surprisingly however, the effect is quantitatively the same for different metals in contact. This is because a pure metal single crystal with a larger elastic modulus generally has, on average, larger dislocation nucleation strength. Larger stresses are therefore required to deform the crystal plastically.

Next we investigate if the plastic properties of two bodies in contact can be mapped to that of a single plastically deformable body. This allows us to determine whether the problem of two plastically deformable bodies in contact can be represented by a simplified equivalent problem composed of a single plastically deformable body in contact with a rigid platen. Elastically both problems are identical as long as the gap geometry and effective elastic modulus of both bodies are the same. Results show that the problem of two plastically deformable bodies in contact can be simplified by treating an equivalent problem. The mapping is possible provided that 1) the source strength in the equivalent problem is that of the softest material in the original problem, and 2) the source density is equal to the sum of the source densities contained in the two deformable crystals.

The static friction behavior of micrometer sized asperities is examined in Chapter 5. Previous discrete dislocation plasticity studies of friction have focused only on contact with a single asperity on top of a large body, and flattened at a constant depth. The behavior of multi-asperity contact is different from single asperity contact since it is easier to shear closely spaced asperities. Here, we analyze the static friction of a body with a sinusoidal surface in contact with a platen pre-loaded with a constant normal force, and investigate how the friction force and the friction coefficient vary with the applied normal force.

The friction force is found to be independent of whether the platen is rigid, or elastic. This holds even for a plastic platen, as long as the plastic properties of both bodies in contact are the same. Both the friction force and friction coefficient decrease when the applied normal force is increased. The local friction coefficient is also highly non-uniform, and it can be a few times larger than the average friction coefficient. When the asperity size is decreased, the friction force and the friction coefficient increase, due to the size dependence of plasticity during flattening.

Finally some concluding remarks and recommendations are given in Chapter 6.

SAMENVATTING

Het werk dat gepresenteerd wordt in dit proefschrift heeft tot doel een beter begrip te verkrijgen van het mechanisch gedrag van twee metalen objecten (lichamen) in contact, die beiden plastisch kunnen deformeren door beweging van dislocaties. De analyse is een uitbreiding van eerdere contact-studies, die één plastisch deformeerbaar lichaam in contact met een starre plaat beschouwden. In deze studie wordt het contact tussen een lichaam met een sinusoïdaal oppervlak met golflengte op micrometer-schaal en een plaat beschouwd. Dit is de schaal waarop bekend is dat plasticiteit grootte-afhankelijk is.

De simulaties zijn uitgevoerd met de discrete dislocatie plasticiteit-methode (DDP-methode), die micronschaal-plasticiteit accuraat beschrijft en grootte-effecten kan voorspellen. Plasticiteit wordt beschreven als de collectieve beweging van discrete dislocaties, de dragers van plasticiteit. De dislocaties worden gemodelleerd als lijnsingulariteiten in een verder isotroop lineair elastisch medium. Hierdoor bevat het model de karakteristieke lengteschaal van plasticiteit, de Burgersvector, waardoor het model grootte-effecten in de plasticiteit in rekening kan brengen.

De nieuwe formulering wordt beschreven in hoofdstuk 2. Het contact tussen twee lichamen met randdislocaties wordt behandeld als een probleem met randvoorwaarden, en de oplossing voor de image-velden wordt verkregen door de potentiële energie van beide kristallen te minimaliseren, terwijl voldaan wordt aan de contactcondities aan het interface.

Alhoewel dit een algemeen toepasbaar model betreft, richten we onze aandacht eerst, in hoofdstuk 3, op het contact tussen een plastisch deformeerbaar lichaam met een sinusoïdaal oppervlak en een starre of elastische plaat. Het verschil met eerdere DDP-contactstudies is dat daarin het effect van een starre plaat is beschreven door een set randvoorwaarden, terwijl in dit werk beide lichamen expliciet gemodelleerd zijn. Twee limietgevallen worden bekeken, te weten wrijvingsloos contact en contact met volledige hechting. In tegenstelling tot resultaten uit eerdere studies vinden we dat het daadwerkelijke contactoppervlak en daardoor de daadwerkelijke contactdruk sterk beïnvloed worden door de contactconditie. Het schijnbare contactoppervlak, de schijnbare contactdruk en de plastische deformatie in het kristal worden daarentegen niet beïnvloed. De exacte vorm van het daadwerkelijke contactoppervlak beïnvloedt de lokale druk, maar niet het gemiddelde hiervan of het totale plastische gedrag.

In hetzelfde hoofdstuk wordt een grootte-afhankelijke plastische respons aangetoond, waarbij kleine oneffenheden moeilijker te deformeren blijken te zijn dan grotere oneffenheden. Dit is in overeenstemming met eerdere DDP-studies van contacten. Zoals verwacht, vinden we dat het grootte-effect minder uitgesproken is naarmate de compliantie van de plaat hoger is.

De analyse wordt daarna in hoofdstuk 4 uitgebreid met een contact tussen twee lichamen die beide kunnen deformeren. We vinden dat wanneer beide lichamen in contact plastisch deformeren, de plastische respons ook grootte-afhankelijk is. Het is verrassend om te vinden dat dit effect kwantitatief hetzelfde is voor verschillende metalen in contact. Dit komt doordat een enkel metaalkristal met een grotere elastische modulus gemiddeld genomen ook een grotere dislocatie-nucleatiesterkte heeft. Daardoor zijn er ook grotere spanningen nodig om het kristal plastisch te deformeren.

Vervolgens onderzoeken we of de plastische eigenschappen van twee lichamen in contact vertaald kunnen worden naar die van één plastisch deformeerbaar lichaam. Hierdoor zouden we kunnen we nagaan of het probleem van twee plastisch deformeerbare lichamen gerepresenteerd kan worden door één plastisch deformeerbaar lichaam en een starre plaat. Elastisch zijn beide problemen identiek zolang de geometrie van de ruimte tussen de lichamen en de effectieve elastische modulus van beide lichamen hetzelfde zijn. Onze resultaten laten zien dat het probleem van twee plastisch deformeerbare lichamen in contact inderdaad vereenvoudigd kan worden tot een enkelzijdig equivalent probleem. Deze vertaalslag is mogelijk zolang 1) de bronsterkte in het equivalente probleem gelijk is aan die van het zachtste materiaal in het originele probleem en 2) de brondichtheid gelijk is aan de som van brondichtheden in de twee deformeerbare kristallen.

Het statische wrijvingsgedrag van micrometer-grote oneffenheden is onderzocht in hoofdstuk 5. Eerdere DDP-studies van wrijving hebben alleen gekeken naar contact met een enkele oneffenheid bovenop een groot lichaam, afgeplat op een constante niveau. Het gedrag van een contact met veel oneffenheden is anders dan dat van een contact met slechts een enkele oneffenheid, aangezien het makkelijker is om dicht bijelkaar gelegen oneffenheden af te schuiven. We analyseren hier de statische wrijving van een lichaam met een sinusoïdaal oppervlak in contact met een plaat,die voorbelast is met een constante normaalkracht, en onderzoeken hoe de wrijvingskracht en de wrijvingscoëfficiënt variëren met de aangebrachte normale belasting.

De wrijvingskracht is onafhankelijk van de eigenschap of de plaat star of elastisch is. Dit geldt zelfs voor een plastische plaat, zoang de plastische eigenschappen van beide lichamen in contact hetzelfde zijn. Zowel de wrijvingskracht als de wrijvingsconstante nemen af als de aangebrachte normale belasting wordt

verhoogd. De lokale wrijvingscoëfficiënt is in hoge mate niet-uniform en kan enkele malen groter zijn dan de gemiddelde wrijvingscoëfficiënt. Wanneer de grootte van de oneffenheid afneemt, nemen de wrijvingskracht en de wrijvingscoëfficiënt toe, door de grootte-afhankelijkheid van de plasticiteit gedurende het afvlakken.

Tot slot worden in hoofdstuk 6 een aantal conclusies en aanbevelingen gegeven.

1

INTRODUCTION

Kelvin NG WEI SIANG

The increase of scientific knowledge lies
not only in the milestones of science,
but in the efforts of the very large body of men,
who with love and devotion,
observe and study nature.

Polykarp Kusch

Science never solves a problem without creating ten more.

George Bernard Shaw

1

1.1. GENERAL INTRODUCTION

THE drive to develop compact machines with high performance and functionality has reduced the dimensions of the machines and their internal components down to the micrometer or the nanometer scale [1, 2]. However, as the surface to volume ratio increases with decreasing size, the performance of the machines become increasingly dominated by interfacial forces [3, 4].

One of the direct consequences of contact between the surfaces is friction, defined as the resistance to relative motion between the surfaces. In miniaturized devices, friction and adhesion pose a serious problem as they can completely hamper the device functionality. As a result, many of these devices have low reliability, and they cannot be commercialized [5]. Overcoming friction remains therefore one of the central challenges in the design of reliable micro/nano electromechanical systems (MEMS/NEMS) [6, 7].

Numerous studies (e.g. [8–20]) have been carried out to understand the contact and friction behavior of surfaces in contact. Friction is often quantified by the friction coefficient μ, defined by the ratio of the friction force F_f to the normal force F_y compressing the surfaces together. The coefficient μ is experimentally found to be in the range of 0.1 to 1.4 (see e.g. [21, 22]), but different relationships between F_f, F_y and μ have been obtained. Several experiments demonstrate that the friction force is proportional to the applied normal force, and hence the friction coefficient μ is independent of F_y [8–12]. However, other studies report that the friction coefficient decreases with increasing applied normal force [13–20], similarly to a Hertzian contact. It is not yet completely understood what causes

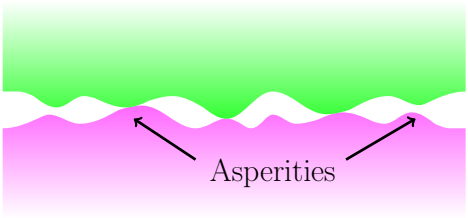

Figure 1.1: Asperities, or protrusions of a surface, of various sizes. Some are in contact.

the different contact behavior, since the results are strongly dependent on the specific testing condition. What is certain is that for highly adhesive surfaces in contact [23], the contact behavior and friction are dependent on the material plastic properties. This is because the contact pressure is usually large enough to induce plastic deformation in the asperities [24–26], or protrusions of a surface (Fig. 1.1).

To investigate the effect of plastic deformation on the contact behavior, models using continuum mechanics theories have been developed, which consider

the deformation of individual asperities of a rough surface (e.g. [27–30]). One of the earliest rough surface contact model is introduced by Greenwood and Williamson [27]. They assume all asperities to be identical and spherical, and the asperity heights are exponentially distributed (Fig. 1.2). The elastic deformation

Figure 1.2: An idealized surface by Greenwood and Williamson, composed of identical hemispherical asperities of radius r, but with different heights.

of each asperity is treated as a non-interacting Hertzian spherical contact, which gives $A \propto F_y^{2/3}$ [31]. Plastic yield is based on the Von-Mises criterion [32, 33], and the yield strength is assumed a material property. Several rough surface contact models (e.g. [30, 34, 35]) also used the same approach for constructing the surface, but with different statistical distributions of asperity geometries, e.g. asperity heights and curvatures. However, later experimental studies show that the curvature of the asperities measured depends strongly on the resolution of the surface measuring instrument [36–38]. To describe the surfaces more accurately

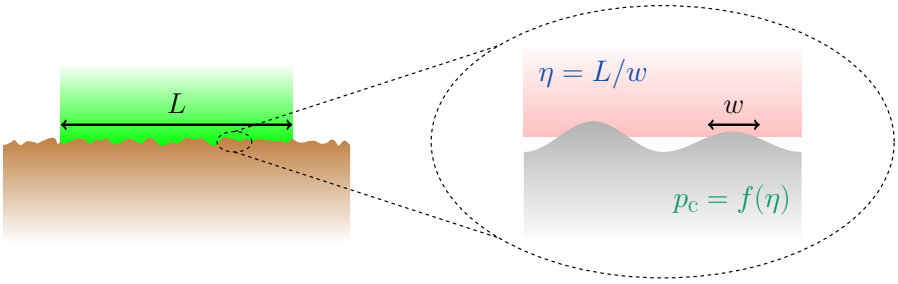

Figure 1.3: Right: complete contact at length scale L, and left: contact at a smaller length scale w when the surface is magnified.

Persson [39] developed a contact theory which considers the contact pressure as a function of a parameter $\eta = L/w$, where L is the length scale of the complete contact and w is the length scale of contact of the surface when magnified (see Fig. 1.3). No contact length scales are therefore excluded in the analysis. In all these continuum studies, the normal force F_y is found to vary linearly with the true contact area A_c, although the proportionality constant differs [40].

To investigate directly how the friction force varies with the applied normal force, Chang *et al.* [41] presented a static friction model which treats the static friction force as the shear force corresponding to the onset of plasticity of the asperities. Contact is assumed full stick. Later works [42–45] modify the contact

model to include the transition from the onset of plasticity to full plastic deformation [42, 46], so to account for the fact that the asperities support additional shear load after plasticity sets in. These studies found that when dissipation occurs by plasticity the friction coefficient μ decreases when the applied normal force is increased. The reason is that the stresses induced by the normal force facilitate plastic shearing.

The relationship between the friction force, hence friction coefficient with the normal load differs however between the different local continuum plasticity contact studies (compare e.g. [42] and [44]). Local continuum models lack also a characteristic length scale to capture size effects [47]. Micro compression tests on pillars reveal a plasticity size effect at the (sub)-micron scale [48–51], i.e. the contact pressure required to deform smaller pillars is larger. This is because plasticity sets in at larger strains for smaller sized asperities. A larger normal force and tangential force are thus required to deform the asperities then what would be predicted by a continuum model, indicating that the contact pressure, friction force, and the friction coefficient could be underestimated. To predict how much these quantities would be under-estimated, plasticity size effects must be accounted for when modeling the contact behavior of micrometer sized asperities.

Although molecular dynamics simulations have been used to analyze contact between surfaces [47, 52–54], they are computationally expensive when the contact size is larger than the nanometer scale. To address too the contact problem at the micron scale, studies of flattening [55–58] and shearing [59–62] of micron-sized contacts have been already carried out using discrete dislocation plasticity [63]. This method fills the gap between the atomistic and the macroscopic models, since it averages over the atoms, but accounts for the nucleation and glide of dislocations. Plasticity in the body is described by the collective motion of discrete edge dislocations, and by that the model contains the intrinsic length scale of plasticity: the Burgers vector **b**. Although non-local continuum plasticity models [64–67] have also been developed in recent years to include the effect of dislocations by mean fields, the discrete effects of plastic flow, e.g. source limitation [48, 51], and high local contact pressure peaks are unaccounted for [68].

Results obtained from discrete dislocation plasticity contact studies differ indeed from local continuum plasticity contact studies. For instance size [55, 69] and spacing effects [55, 56] are observed during flattening. A plastically flattened asperity is more compliant, if subsequently sheared [60].

1.2. MOTIVATION

ALTHOUGH the contact behavior of the asperities has been investigated extensively using discrete dislocation plasticity, the analysis have so far focused only on contact between a plastically deformable asperity and a rigid body, for which the effects of the rigid body are mimicked through a set of boundary conditions. To preserve compatibility dislocations are prevented from escaping the contact, causing them to pile up beneath the contact. The question arises on how the contact pressure profiles are affected by this constraint. Also, plasticity size effect and the highly non-uniform contact profiles and pressure observed in discrete dislocation plasticity studies of contact with a rigid body are expected to be different when both bodies in contact are deformable. To understand this a contact model that describes both bodies in contact that can deform by dislocation plasticity is developed in this thesis.

Continuum studies of contact between two deformable bodies has been routinely simplified by treating an equivalent problem where only one body is deformable and the other is rigid [28, 39, 46, 70–73], since the elastic responses are identical provided that the gap geometry and the effective elastic modulus of the bodies remains unchanged [39, 74]. The question arises on whether, and to what extend, the simplification is still valid even when plasticity, size dependent at the (sub)-micron scale, occurs. Here, this question is addressed using the developed two body discrete dislocation plasticity model.

Previous discrete dislocation plasticity studies have focused on analyzing the static friction behavior of a single asperity on top of a large body, where the asperity is pre-loaded by a constant normal displacement [60, 61, 75]. However, the behavior of multi-asperity contact is found to be different from a single asperity contact: in a study of shearing three asperities [60] the contact shear stress is smaller than shearing only a single isolated asperity. In this thesis, we will investigate the static friction response of a multi-asperity contact, when the only dissipation process active is plasticity.

1.3. OBJECTIVES AND STRUCTURE OF THE THESIS

HERE, we present the analysis of flattening and shearing of two bodies in contact that can both deform by dislocation plasticity. The developed formulation that describes both plastically deformable bodies is presented in Chapter 2.

Simulations of contact between a body with micrometer sized sinusoidal asperities and a body with a flat surface (platen) are performed, for which stresses in the material are relaxed by the collective glide of dislocations. In Chapter 3, we examine how the contact conditions affect the plastic response of a metal single crystal with a sinusoidal surface flattened by a rigid body. How the size depen-

dent plastic response is affected by the compliance of the platen is also explored.

Next, contact between two bodies that can both deform by dislocation plasticity is investigated in Chapter 4. For two plastically deformable bodies a size dependent plastic behavior is also observed. Surprisingly however, the effect is quantitatively the same for different metals in contact. This is because a single metal crystal with a larger elastic modulus has on average, larger dislocation nucleation strength. The larger stresses in the crystal with a larger elastic modulus therefore does not lead to more plasticity in the crystal.

The question of whether the problem of two metal crystals in contact can be mapped to an equivalent system, made of a single plastically deformable body in contact with a rigid body, is addressed in the same chapter.

The problem of shear of sinusoidal asperities is dealt with in Chapter 5. Here, a normal force is first applied on the top surface of the platen in contact with the asperities before applying a tangential (shear) displacement. We investigate how the static friction force and the friction coefficient of micron sized sinusoidal asperities vary with the applied normal force. The size dependent behavior of the friction force and the friction coefficient is also explored.

Finally conclusions and recommendations for future research are presented in Chapter 6.

REFERENCES

[1] M. Epicoco, *Knowledge patterns and sources of leadership: Mapping the semiconductor miniaturization trajectory,* Res. Policy **42**, 180 (2013).

[2] J. W. G. Turner, A. Popplewell, R. Patel, T. R. Johnson, N. J. Darnton, S. Richardson, S. W. Bredda, R. J. Tudor, R. Bithell, R. Jackson, and S. M. Remmert, *Ultra boost for economy: extending the limits of extreme engine downsizing,* SAE Int. J. Engines **7**, 387 (2014).

[3] B. Bhushan, *Nanotribology and nanomechanics of MEMS/NEMS and bioMEMS/bioNEMS materials and devices,* Microelectron. Eng. **84**, 387 (2007).

[4] I. Szlufarska, M. Chandross, and R. W. Carpick, *Recent advances in single-asperity nanotribology,* J. Phys. D: Appl. Phys. **41**, 123001 (2008).

[5] M. P. De Boer and T. M. Mayer, *Tribology of MEMS,* MRS Bull. **26**, 302 (2001).

[6] A. D. Romig, M. T. Dugger, and P. J. McWhorter, *Materials issues in microelectromechanical devices: science, engineering, manufacturability and reliability,* Acta Mater. **51**, 5837 (2003).

[7] A. Socoliuc, E. Gnecco, S. Maier, O. Pfeiffer, A. Baratoff, R. Bennewitz, and E. Meyer, *Atomic-scale control of friction by actuation of nanometer-sized contacts,* Science **313**, 207 (2006).

[8] Q. Chen and G. P. Carman, *Microscale tribology (friction) measurement and influence of crystal orientation and fabrication process,* in *Proc. 13th Annu. Int. Conf. Micro Electro Mech. Syst.* (IEEE, 2000) pp. 657–661.

[9] D. Gourdon and J. N. Israelachvili, *Transitions between smooth and complex stick-slip sliding of surfaces,* Phys. Rev. E **68**, 021602 (2003).

[10] A. Socoliuc, R. Bennewitz, E. Gnecco, and E. Meyer, *Transition from stick-slip to continuous sliding in atomic friction: entering a new regime of ultralow friction,* Phys. Rev. Lett. **92**, 134301 (2004).

[11] J. Gao, W. D. Luedtke, D. Gourdon, M. Ruths, J. N. Israelachvili, and U. Landman, *Frictional forces and amontons' law: from the molecular to the macroscopic scale,* J. Phys. Chem. B **108**, 3410 (2004).

[12] L. Bureau, C. Caroli, and T. Baumberger, *Frictional dissipation and interfacial glass transition of polymeric solids,* Phys. Rev. Lett. **97**, 225501 (2006).

[13] U. D. Schwarz, W. Allers, G. Gensterblum, and R. Wiesendanger, *Low-load friction behavior of epitaxial c 60 monolayers under hertzian contact,* Phys. Rev. B **52**, 14976 (1995).

[14] R. W. Carpick and M. Salmeron, *Scratching the surface: fundamental investigations of tribology with atomic force microscopy,* Chem. Rev. **97**, 1163 (1997).

[15] P. J. Blau, *The significance and use of the friction coefficient,* Tribol. Int. **34**, 585 (2001).

[16] O. Ben-David and J. Fineberg, *Static friction coefficient is not a material constant,* Phys. Rev. Lett. **106**, 254301 (2011).

[17] Y. Katano, K. Nakano, M. Otsuki, and H. Matsukawa, *Novel friction law for the static friction force based on local precursor slipping,* Sci. Rep. **4** (2014).

[18] E. Rabinowicz, *Friction coefficients of noble metals over a range of loads,* Wear **159**, 89 (1992).

[19] I. Etsion and M. Amit, *The effect of small normal loads on the static friction coefficient for very smooth surfaces,* J. Tribol. T. ASME. **115**, 406 (1993).

[20] A. Ovcharenko, G. Halperin, and I. Etsion, *Experimental study of adhesive static friction in a spherical elastic-plastic contact,* J. Tribol. T. ASME. **130**, 021401 (2008).

[21] P. J. Blau, *Experimental aspects of friction research on the macroscale,* in *Fundamentals of Tribology and Bridging the Gap Between the Macro-and Micro/Nanoscales* (Springer, 2001) pp. 261–278.

[22] F. Cardarelli, *Materials handbook: a concise desktop reference* (Springer Science & Business Media, 2008).

[23] L. Vitos, A. V. Ruban, H. L. Skriver, and J. Kollar, *The surface energy of metals,* Surf. Sci. **411**, 186 (1998).

[24] F. P. Bowden and D. Tabor, *The nature of sliding and the analysis of friction,* Proc. R. Soc. London, Ser. A **169**, 371 (1939).

[25] S. Hyun, L. Pei, J. F. Molinari, and M. O. Robbins, *Finite-element analysis of contact between elastic self-affine surfaces,* Phys. Rev. E **70**, 026117 (2004).

[26] R. Jedynak and M. Sułek, *Numerical and experimental investigation of plastic interaction between rough surfaces,* Arab J. Sci. Eng. **39**, 4165 (2014).

[27] J. A. Greenwood and J. B. P. Williamson, *Contact of nominally flat surfaces,* R. Soc. Lond. Proc. Ser. A Math. Phys. Eng. Sci. **295**, 300 (1966).

[28] A. Majumdar and B. Bhushan, *Fractal model of elastic-plastic contact between rough surfaces,* J. Tribol. T. ASME. **113**, 1 (1991).

[29] B. N. J. Persson, *Contact mechanics for randomly rough surfaces,* Surf. Sci. Rrp. **61**, 201 (2006).

[30] R. L. Jackson and J. L. Streator, *A multi-scale model for contact between rough surfaces,* Wear **261**, 1337 (2006).

[31] H. Hertz, *Über die berührung fester elastischer körper,* J. Reine Angew. Math. **92**, 156 (1882).

[32] R. V. Mises, *Mechanik der festen körper im plastisch-deformablen zustand,* Gött. Nachr. Math. Phys. Klasse **1913**, 582 (1913).

[33] R. Hill, *The mathematical theory of plasticity*, Vol. 11 (Oxford university press, 1998).

[34] A. W. Bush, R. D. Gibson, and T. R. Thomas, *The elastic contact of a rough surface,* Wear **35**, 87 (1975).

[35] J. A. Greenwood, *A simplified elliptic model of rough surface contact,* Wear **261**, 191 (2006).

[36] A. W. Bush, R. D. Gibson, and G. P. Keogh, *The limit of elastic deformation in the contact of rough surfaces,* Mech. Res. Commun. **3**, 169 (1976).

[37] P. I. Oden, A. Majumdar, B. Bhushan, A. Padmanabhan, and J. J. Graham, AFM *imaging, roughness analysis and contact mechanics of magnetic tape and head surfaces,* J. Tribol. T. ASME. **114**, 666 (1992).

[38] M. Klüpper and G. Heinrich, *Rubber friction on self-affine road tracks,* Rubber Chem. Technol. **73**, 578 (2000).

[39] B. N. J. Persson, *Elastoplastic contact between randomly rough surfaces,* Phys. Rev. Lett. **87**, 116101 (2001).

[40] G. Carbone and F. Bottiglione, *Contact mechanics of rough surfaces: a comparison between theories,* Meccanica **46**, 557 (2011).

[41] W. R. Chang, I. Etsion, and D. B. Bogy, *Static friction coefficient model for metallic rough surfaces,* J. Tribol. T. ASME. **110**, 57 (1988).

[42] L. Kogut and I. Etsion, *A semi-analytical solution for the sliding inception of a spherical contact,* J. Tribol. T. ASME. **125**, 499 (2003).

[43] L. Kogut and I. Etsion, *A static friction model for elastic-plastic contacting rough surfaces,* J. Tribol. T. ASME. **126**, 34 (2004).

[44] V. Brizmer, Y. Kligerman, and I. Etsion, *Elastic–plastic spherical contact under combined normal and tangential loading in full stick,* Tribol. Lett. **25**, 61 (2007).

[45] I. Etsion, *Revisiting the cattaneo–mindlin concept of interfacial slip in tangentially loaded compliant bodies,* J. Tribol. T. ASME. **132**, 020801 (2010).

[46] L. Kogut and I. Etsion, *Elastic-plastic contact analysis of a sphere and a rigid flat,* J. Appl. Mech. **69**, 657 (2002).

[47] B. Luan and M. O. Robbins, *The breakdown of continuum models for mechanical contacts,* Nature **435**, 929 (2005).

[48] J. R. Greer, W. C. Oliver, and W. D. Nix, *Size dependence of mechanical properties of gold at the micron scale in the absence of strain gradients,* Acta Mater. **53**, 1821 (2005).

[49] L. Nicola, Y. Xiang, J. J. Vlassak, E. Van der Giessen, and A. Needleman, *Plastic deformation of freestanding thin films: experiments and modeling,* J. Mech. Phys. Solids **54**, 2089 (2006).

[50] D. Kiener, W. Grosinger, G. Dehm, and R. Pippan, *A further step towards an understanding of size-dependent crystal plasticity: In situ tension experiments of miniaturized single-crystal copper samples,* Acta Mater. **56**, 580 (2008).

[51] J. R. Greer and J. T. M. De Hosson, *Plasticity in small-sized metallic systems: Intrinsic versus extrinsic size effect,* Prog. Mater. Sci. **56**, 654 (2011).

[52] M. Chandross, C. D. Lorenz, M. J. Stevens, and G. S. Grest, *Simulations of nanotribology with realistic probe tip models,* Langmuir **24**, 1240 (2008).

[53] G. Gao, R. J. Cannara, R. W. Carpick, and J. A. Harrison, *Atomic-scale friction on diamond: a comparison of different sliding directions on (001) and (111) surfaces using* MD *and* AFM*,* Langmuir **23**, 5394 (2007).

[54] Y. Mo, K. T. Turner, and I. Szlufarska, *Friction laws at the nanoscale,* Nature **457**, 1116 (2009).

[55] F. Sun, E. Van der Giessen, and L. Nicola, *Plastic flattening of a sinusoidal metal surface: a discrete dislocation plasticity study,* Wear **296**, 672 (2012).

[56] F. Sun, E. Van der Giessen, and L. Nicola, *Interaction between neighboring asperities during flattening: a discrete dislocation plasticity analysis,* Mech. Mater. **90**, 157 (2015).

[57] K. Ng Wei Siang and L. Nicola, *Discrete dislocation plasticity analysis of contact between deformable bodies with simple geometry,* Model. Simul. Mater. Sci. **24**, 045008 (2016).

[58] K. Ng Wei Siang and L. Nicola, *Contact between two plastically deformable crystals: a discrete dislocation dynamics study,* submitted to Philos. Mag. (2016).

[59] V. S. Deshpande, A. Needleman, and E. Van der Giessen, *Discrete dislocation plasticity analysis of static friction,* Acta Mater. **52**, 3135 (2004).

[60] F. Sun, E. Van der Giessen, and L. Nicola, *Effect of plastic flattening on the shearing response of metal asperities: a dislocation dynamics analysis,* J. Appl. Mech. **82**, 071009 (2015).

[61] R. J. Dikken, E. Van der Giessen, and L. Nicola, *Plastic shear response of a single asperity: A discrete dislocation plasticity analysis,* Philos. Mag. (2015).

[62] K. Ng Wei Siang and L. Nicola, *Static friction of sinusoidal surfaces: a discrete dislocation plasticity analysis,* submitted to Acta Mater. (2016).

[63] E. Van der Giessen and A. Needleman, *Discrete dislocation plasticity: a simple planar model,* Model. Simul. Mater. Sci. **3**, 689 (1995).

[64] N. A. Fleck, G. M. Muller, M. F. Ashby, and J. W. Hutchinson, *Strain gradient plasticity: theory and experiment,* Acta Metall. Mater. **42**, 475 (1994).

[65] H. Gao and Y. Huang, *Geometrically necessary dislocation and size-dependent plasticity,* Scr. Mater. **48**, 113 (2003).

[66] Y. S. Chen, W. Choi, S. Papanikolaou, M. Bierbaum, and J. P. Sethna, *Scaling theory of continuum dislocation dynamics in three dimensions: Self-organized fractal pattern formation,* Int. J. Plas. **46**, 94 (2013).

[67] S. Sandfeld and G. Po, *Microstructural comparison of the kinematics of discrete and continuum dislocations models,* Model. Simul. Mater. Sci. **23**, 085003 (2015).

[68] A. Needleman and E. Van der Giessen, *Discrete dislocation and continuum descriptions of plastic flow,* Mater. Sci. Eng. A **309**, 1 (2001).

[69] L. Nicola, A. F. Bower, K. S. Kim, A. Needleman, and E. Van Der Giessen, *Multi-asperity contact: a comparison between discrete dislocation and crystal plasticity predictions,* Philos. Mag. **88**, 3713 (2008).

[70] W. R. Chang, I. Etsion, and D. B. Bogy, *An elastic-plastic model for the contact of rough surfaces,* J. Tribol. T. ASME. **109**, 257 (1987).

[71] W. Yan and K. Komvopoulos, *Contact analysis of elastic-plastic fractal surfaces,* J. Appl. Phys. **84**, 3617 (1998).

[72] L. Kogut and I. Etsion, *A finite element based elastic-plastic model for the contact of rough surfaces,* Tribol. Trans. **46**, 383 (2003).

[73] L. Pastewka and M. O. Robbins, *Contact between rough surfaces and a criterion for macroscopic adhesion,* Proc. Natl. Acad. Sci. U.S.A. **111**, 3298 (2014).

[74] K. L. Johnson, *Contact Mechanics* (Cambridge University Press, 1987).

[75] H. Song, R. J. Dikken, L. Nicola, and E. Van der Giessen, *Plastic ploughing of a sinusoidal asperity on a rough surface,* J. Appl. Mech. **82**, 071006 (2015).

2

COMPUTATIONAL APPROACH

Your assumptions are your windows on the world.
Scrub them off every once in a while, or the light won't come in.

Isaac Asimov

Parts of this chapter have been published in Model. Simul. Mater. Sci. **24**, 045008 (2016) [1].

2

The approach to determine the deformation of two bodies in contact with a given dislocation distribution is described in this chapter. The model intends to improve on previous dislocation dynamics models which consider contact between a deformable body and a rigid body, and the effect of the rigid body is mimicked through boundary conditions. The linear elastic deformation fields are given as the sum of two linearly additive fields: the dislocation fields and the image fields. The dislocation fields are analytical fields of the edge dislocations present in each body as if each body containing them were infinite. The image fields enforce the boundary and contact conditions of the bodies in contact. Given that the image fields are non-singular they are obtained by solving the contact problem using the Finite Element Method. The fields of the dislocations in both bodies are then verified for the two body contact model, by comparing with those obtained by the traditional single body discrete dislocation plasticity model. Finally, the constitutive rules governing dislocation dynamics are briefly described.

2.1. INTRODUCTION

IN this chapter the formulation used to describe the contact between two bodies that can deform plastically is presented [1]. First it is described how at each time increment the stress and displacement fields of both crystals in contact containing dislocations are obtained. Next, a description of the constitutive rules that govern the dynamics of the dislocations follows.

2.2. ELASTIC CONTACT PROBLEM

WE first consider two linear elastic bodies. Following Wriggers [2], contact between the bodies is treated as a constrained minimization problem. Each body i has domain $\Omega^{(i)}$ bounded by a boundary $\Gamma^{(i)}$ where $\Gamma^{(1)} \cap \Gamma^{(2)} = \gamma_c$ and γ_c is the contact surface. The total potential energy functional Π^P for two elastic bodies in contact, without frictional sliding and neglecting body forces, is given as

$$\Pi^P(\mathbf{u}) = \sum_{i=1}^{2} \left\{ \frac{1}{2} \int_{\Omega^{(i)}} \left[\boldsymbol{\varepsilon}(\mathbf{u})^T \boldsymbol{\sigma}(\mathbf{u}) \right]^{(i)} d\Omega - \int_{\Gamma_\sigma^{(i)}} \mathbf{u}^{(i)T} \mathbf{t}^{(i)} d\Gamma \right\} + \Pi^C(\mathbf{u}), \tag{2.1}$$

where $\boldsymbol{\varepsilon}$ and $\boldsymbol{\sigma}$ are the strain and stress tensors, $\mathbf{u}$ are the displacement vector fields, and $\mathbf{t}^{(i)}$ are the tractions acting on the boundary $\Gamma_\sigma^{(i)}$. Following the the penalty method, the constraint energy term Π^C has the objective of minimizing penetration between the contact surfaces. For two dimensional contact problems considered in this work, Π^C is expressed as

$$\Pi^C(\mathbf{u}) = \frac{1}{2} \int_{\gamma_c} \left[\epsilon_n g_n^2(\mathbf{u}) + \epsilon_t g_t^2(\mathbf{u}) \right] d\Gamma, \quad \text{with } \epsilon_n, \epsilon_t \geq 0, \tag{2.2}$$

where the normal gap function g_n and the tangential gap function g_t are as described in the following subsection. The penalty parameters in the normal and tangential directions of the surface of body 1 in Eq. (2.2) are ϵ_n and ϵ_t. For frictionless contact, $\epsilon_n \to \infty, \epsilon_t = 0$, whereas for full stick contact, $\epsilon_n, \epsilon_t \to \infty$. The potential energy functional minimum is obtained by equating the first variation of Π^P to zero [2, 3],

$$\begin{aligned} &\sum_{i=1}^{2} \left\{ \int_{\Omega^{(i)}} \left[\delta\boldsymbol{\varepsilon}(\mathbf{u})^T \boldsymbol{\sigma}(\mathbf{u}) \right]^{(i)} d\Omega - \int_{\Gamma_\sigma^{(i)}} \delta\mathbf{u}^{(i)T} \mathbf{t}^{(i)} d\Gamma \right\} \\ &+ \underbrace{\int_{\gamma_c} \left[\epsilon_n \delta g_n(\mathbf{u}) g_n(\mathbf{u}) + \epsilon_t \delta g_t(\mathbf{u}) g_t(\mathbf{u}) \right] d\Gamma}_{\Pi^C(\mathbf{u})} = 0. \end{aligned} \tag{2.3}$$

2.2.1. CONTACT KINEMATICS

Following Wriggers [2], to determine contact, the distance between two points

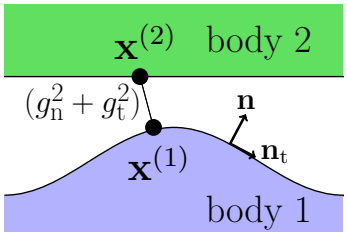

Figure 2.1: Distance between two points on opposite surfaces, described through gap functions (see e.g. [2]).

$\mathbf{x}^{(1)}$ and $\mathbf{x}^{(2)}$ must be defined (Fig. 2.1), as

$$g_{\mathrm{n}} = \left(\mathbf{x}^{(2)} - \mathbf{x}^{(1)}(\boldsymbol{\xi})\right)^{\mathrm{T}} \mathbf{n}^{(1)}, \quad g_{\mathrm{t}_j} = \left(\mathbf{x}^{(2)} - \mathbf{x}^{(1)}(\boldsymbol{\xi})\right)^{\mathrm{T}} \mathbf{n}^{(1)}_{\mathrm{t}_j}, \quad j = 1,2. \tag{2.4}$$

Here $\mathbf{x}^{(i)}$, where $\mathbf{x}^{(i)} = \mathbf{u}^{(i)} + \mathbf{x}_0^{(i)}$, is the coordinate of a point on the surface of body i in the current configuration; $\mathbf{u}^{(i)}$ is the displacement and $\mathbf{x}_0^{(i)}$ is in the original configuration; $\boldsymbol{\xi} = (\xi_{\mathrm{t}_1}, \xi_{\mathrm{t}_2})$ are the curvilinear coordinates of the surface of body 1; and $\mathbf{n}^{(1)}$ and $\mathbf{n}^{(1)}_{\mathrm{t}_j}$ are the normal and tangential unit vectors in the j direction of the two dimensional surface of body 1. The normal unit vector $\mathbf{n}^{(1)}$ is related to $\mathbf{n}^{(1)}_{\mathrm{t}_j}$ via

$$\mathbf{n}^{(1)} = \frac{\mathbf{n}^{(1)}_{\mathrm{t}_1} \times \mathbf{n}^{(1)}_{\mathrm{t}_2}}{||\mathbf{n}^{(1)}_{\mathrm{t}_1} \times \mathbf{n}^{(1)}_{\mathrm{t}_2}||}. \tag{2.5}$$

Given that the contact boundary is locally convex, every point $\mathbf{x}^{(2)}$ forms a contact pair with point $\mathbf{x}^{(1)}(\boldsymbol{\xi})$, determined via the minimum distance problem with the necessary condition

$$\frac{\mathrm{d}}{\mathrm{d}\xi_{\mathrm{t}_j}} ||g(\xi_{\mathrm{t}_1}, \xi_{\mathrm{t}_2})|| = \frac{\mathbf{x}^{(2)} - \mathbf{x}^{(1)}(\xi_{\mathrm{t}_1}, \xi_{\mathrm{t}_2})}{||\mathbf{x}^{(2)} - \mathbf{x}^{(1)}(\xi_{\mathrm{t}_1}, \xi_{\mathrm{t}_2})||} \cdot \mathbf{x}^{(1)}_{,\mathrm{t}_j}(\xi_{\mathrm{t}_1}, \xi_{\mathrm{t}_2}) = 0, \quad j = 1,2. \tag{2.6}$$

Once the contact pair is obtained, contact between the surfaces can be enforced by subjecting the normal gap function g_{n} to the inequality constraint:

$$g_{\mathrm{n}} = \left(\mathbf{x}^{(2)} - \mathbf{x}^{(1)}\right)^{\mathrm{T}} \mathbf{n}^{(1)} \geq 0. \tag{2.7}$$

2.3. DISCRETE DISLOCATION PLASTICITY OF TWO BODIES IN CONTACT

To describe two bodies in contact that can deform by dislocation plasticity, the linear elastic displacement fields $\mathbf{u}^{(i)}$ in each body i, without any loss of generality, is decomposed into two additive linear elastic fields: $\tilde{\mathbf{u}}^{(i)}$ and $\hat{\mathbf{u}}^{(i)}$ [1]. The dislocation displacement fields $\tilde{\mathbf{u}}^{(i)}$ are the analytical fields of the edge dislocations

present in body i as if the body containing them is infinite. The displacement fields $\hat{\mathbf{u}}^{(i)} = \mathbf{u}^{(i)} - \tilde{\mathbf{u}}^{(i)}$ become the new unknown in Eq. (2.3).

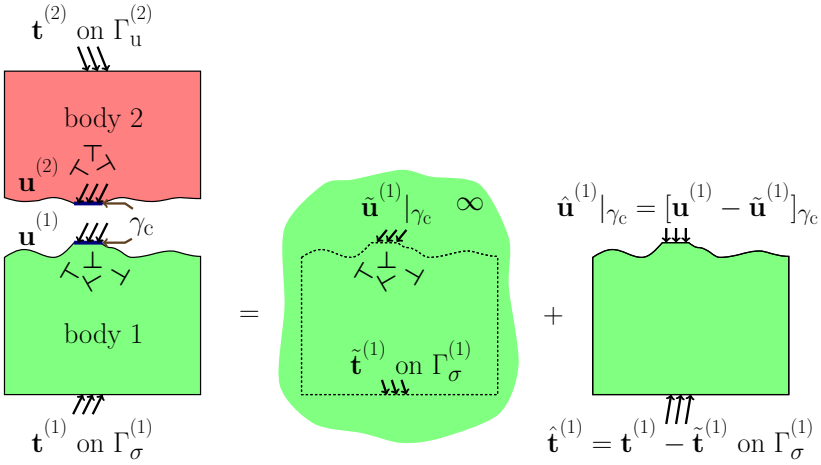

Figure 2.2: Decomposition of a contact plasticity problem. For simplicity of representation, the decomposition of the displacement fields is only presented for body 1. The same decomposition method is used for the fields in body 2. Contact is full stick.

Figure 2.2 gives a schematic representation of the decomposition of displacement and traction fields for body 1 containing dislocations in full stick contact with body 2. The decomposition of the fields is analogous for body 2. Notice that $\hat{\mathbf{u}}^{(i)}$ fields are unique and represent the dislocation images field of the bodies in contact. We have used here the same field decomposition as proposed by Van der Giessen and Needleman for boundary value problems [4], and therefore used the same notation for dislocation fields and image fields.

Replacing $\mathbf{u}$ with $\tilde{\mathbf{u}}^{(i)} + \hat{\mathbf{u}}^{(i)}$ in Eq. (2.3) we obtain

$$\sum_{i=1}^{2} \int_{\Omega^{(i)}} \left[\delta\boldsymbol{\varepsilon}\left(\tilde{\mathbf{u}}+\hat{\mathbf{u}}\right)^{\mathrm{T}} \boldsymbol{\sigma}\left(\tilde{\mathbf{u}}+\hat{\mathbf{u}}\right) \right]^{(i)} \mathrm{d}\Omega + \tag{2.8}$$

$$\int_{\gamma_c} \left[\epsilon_n \, \delta g_n\left(\tilde{\mathbf{u}}+\hat{\mathbf{u}}\right) g_n\left(\tilde{\mathbf{u}}+\hat{\mathbf{u}}\right) + \epsilon_t \, \delta g_t\left(\tilde{\mathbf{u}}+\hat{\mathbf{u}}\right) g_t\left(\tilde{\mathbf{u}}+\hat{\mathbf{u}}\right) \right] \mathrm{d}\Gamma = \sum_{i=1}^{2} \int_{\Gamma_\sigma^{(i)}} \delta\left(\tilde{\mathbf{u}}+\hat{\mathbf{u}}\right)^{(i)\mathrm{T}} \mathbf{t}^{(i)} \, \mathrm{d}\Gamma.$$

Since the $\tilde{\mathbf{u}}^{(i)}$ fields are smooth we can express Eq. (2.8) in discretized form using the Finite Element Method. The discretization of the second integral term is briefly shown here. The gap functions and their first variation are first dis-

cretized, giving

$$g_{\mathrm{n}}^{\mathrm{h}} = \sum_{k}^{n_{\mathrm{c}}} N_k(\zeta)\, g_{\mathrm{n}_k}, \quad g_{\mathrm{t}}^{\mathrm{h}} = \sum_{k}^{n_{\mathrm{c}}} N_k(\zeta)\, g_{\mathrm{t}_k} \tag{2.9}$$
$$\delta g_{\mathrm{n}}^{\mathrm{h}} = \sum_{k}^{n_{\mathrm{c}}} \delta N_k(\zeta)\, g_{\mathrm{n}_k}, \quad \delta g_{\mathrm{t}}^{\mathrm{h}} = \sum_{k}^{n_{\mathrm{c}}} \delta N_k(\zeta)\, g_{\mathrm{t}_k}.$$

Superscript h indicates an approximation of the quantity across the contact surface discretized with n_{c} nodes using finite elements, N are linear shape functions, and ζ is the convective coordinate of the surface. Here, the same shape functions are used for both the normal and tangential gap functions. Using Eq. (2.9) together with Eq. (2.4), the second integral term of Eq. (2.8) becomes

$$\int_{\gamma_{\mathrm{c}}^{\mathrm{h}}} \left[\epsilon_{\mathrm{n}}\, \delta g_{\mathrm{n}}^{\mathrm{h}}\big(\tilde{\mathbf{u}}+\hat{\mathbf{u}}\big) g_{\mathrm{n}}^{\mathrm{h}}\big(\tilde{\mathbf{u}}+\hat{\mathbf{u}}\big) + \epsilon_{\mathrm{t}} \delta g_{\mathrm{t}}^{\mathrm{h}}\big(\tilde{\mathbf{u}}+\hat{\mathbf{u}}\big)\, g_{\mathrm{t}}^{\mathrm{h}}\big(\tilde{\mathbf{u}}+\hat{\mathbf{u}}\big) \right] \mathrm{d}\Gamma = \tag{2.10}$$
$$\sum_{k}^{n_{\mathrm{c}}} \delta\big(\tilde{\mathbf{u}}+\hat{\mathbf{u}}\big)_k \cdot \int_{\gamma_{\mathrm{c}}^{\mathrm{h}}} \Big(\mathbf{C}\cdot\boldsymbol{\epsilon}\cdot\mathbf{C}^{\mathbf{T}}\Big)_k \mathrm{d}\Gamma \cdot \big(\tilde{\mathbf{u}}+\hat{\mathbf{u}}+\mathbf{x}_0\big)_k.$$

The matrix $\mathbf{C}$ contains the shape functions, and $\boldsymbol{\epsilon}$ is a diagonal matrix comprising the penalty parameters. Expressing the remaining terms of Eq. (2.8) in discretized form, and assembling the stiffness of all the elements, we obtain

$$\mathbf{K}(\tilde{\mathbf{u}}^* + \hat{\mathbf{u}}^*) + \mathbf{K}^{\mathrm{P}}(\tilde{\mathbf{u}}^* + \hat{\mathbf{u}}^* + \mathbf{x_0}^*) = \mathbf{f}^{\mathrm{ext}}, \tag{2.11}$$

where nodal vector quantities are indicated by an asterisk; $\mathbf{K}$ and $\mathbf{K}^{\mathrm{P}}$ are the body stiffness matrix and penalty contact stiffness matrix, respectively; and $\mathbf{f}^{\mathrm{ext}}$ is the external nodal force vector. The contact stiffness matrix $\mathbf{K}^{\mathrm{P}}$ is non-zero only at γ_{c}. Equation (2.11) is solved iteratively to obtain $\hat{\mathbf{u}}^{(i)}$; while satisfying the contact constraints; $g_{\mathrm{n}} < 0$ for frictionless contact, and $g_{\mathrm{n}} < 0$, $g_{\mathrm{t}} \to 0$ for full stick contact, and the boundary conditions:

$$\hat{\mathbf{t}}^{(i)} = \mathbf{t}^{(i)} - \tilde{\mathbf{t}}^{(i)} \quad \text{on}\, \Gamma_{\sigma}^{(i)}; \qquad \hat{\mathbf{u}}^{(i)} = \mathbf{u}^{(i)} - \tilde{\mathbf{u}}^{(i)} \quad \text{on}\, \Gamma_{\mathrm{u}}^{(i)}. \tag{2.12}$$

The external displacements are applied on the boundary $\Gamma_{\mathrm{u}}^{(i)}$. At each time increment, $\mathbf{u}$, $\boldsymbol{\epsilon}$ and $\boldsymbol{\sigma}$ in the crystals are given as the sum of the dislocations fields ($\tilde{.}$) and the image fields ($\hat{.}$),

$$\mathbf{u} = \hat{\mathbf{u}} + \tilde{\mathbf{u}}, \quad \boldsymbol{\epsilon} = \hat{\boldsymbol{\epsilon}} + \tilde{\boldsymbol{\epsilon}}, \quad \boldsymbol{\sigma} = \hat{\boldsymbol{\sigma}} + \tilde{\boldsymbol{\sigma}}. \tag{2.13}$$

2.4. VERIFICATION OF STRESS AND DISPLACEMENT FIELDS

HERE, it is verified that the newly proposed two body model correctly captures the dislocation stress fields through the contact. To this end, two rectangular bodies are brought into contact. Each body contains two dislocations

on different slip planes at a fixed location, and each dislocation forms a dipole with the other dislocation in the other body. Contact is full stick. The resulting stress fields are compared with those of an equivalent problem solved by classical discrete dislocation plasticity: normal loading of a single body containing dislocations at the same location as the two body problem. The Burgers vector is taken ten times larger than the Burgers vector **b** of Al to amplify the fields exerted by the dipole. The stress σ_{22} and the vertical displacement u_y are shown in Fig. 2.3 for both cases.

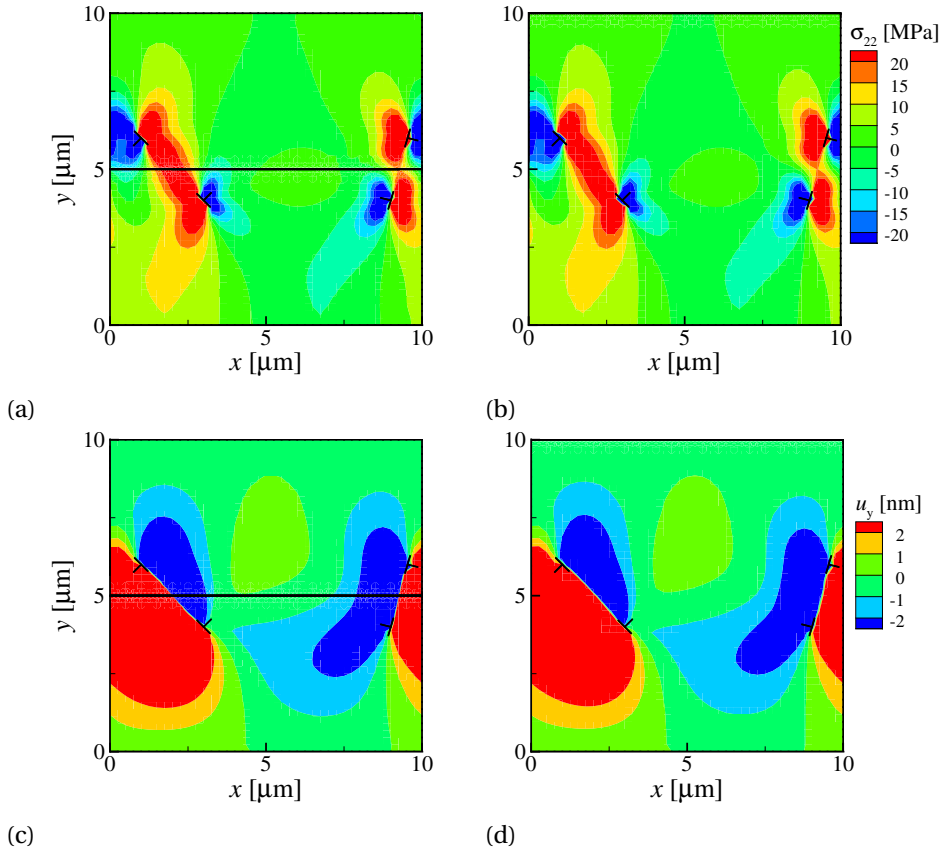

Figure 2.3: Stress σ_{22} distribution for dislocations at the same positions in (a) two bodies in full contact, and (b) single body. The boundary of each body is traced with a black line. The corresponding vertical displacement u_y distribution for (c) two bodies, and (d) single body.

The stresses σ_{22} and the vertical displacements u_y show very good agreement between the two cases. This is also verified for the other stress components, i.e. σ_{11} and σ_{12}, and the horizontal displacements u_x (not shown here).

2.5. DISLOCATION DYNAMICS

DISLOCATION DYNAMICS are modeled by constitutive rules that govern dislocation nucleation, pinning at/depinning from obstacles, annihilation and glide along slip planes. These rules are briefly described here. The reader is referred to [4, 5] for more details.

Three potentially active sets of slip planes are considered based on the two dimensional representation of the FCC crystal structure [6], for which the slip planes are oriented at $\theta_k = \theta_1 + 60(k-1)$; $k \leq 3$, and $\theta_1 = 0°$, unless otherwise stated. Heterogeneous dislocation sources of Frank-Read character and obstacles are randomly distributed along the slip planes throughout the initially dislocation and stress free bodies. The spacing between slip planes with the same orientation is $200\,b$, where b is the Burgers vector.

A dislocation dipole nucleates when the resolved shear stress τ exerted on a dislocation source exceeds its critical strength τ_{nuc} over a certain time interval t_{nuc}. The nucleation length L_{nuc} for each dipole is given by

$$L_{\text{nuc}} = \frac{\mu b}{2\pi(1-\nu)\tau_{\text{nuc}}}, \tag{2.14}$$

where μ and ν are the shear modulus and Poisson's ratio of the material respectively. If dislocations of opposite signs (dipole) approach each other too closely on the same slip plane they will annihilate.

Glide of the dislocations in the crystal is governed by a simple constitutive equation which relates the velocity v^i of dislocation i to the resolved Peach Koehler force f^i_{p}:

$$v^i = f^i_{\text{p}}/D, \quad f^i_{\text{p}} = \Big(\sum_{j\neq i} \tilde{\sigma}^j_{lk} + \hat{\sigma}^i_{lk}\Big) b^i_k m_l, \tag{2.15}$$

where $\tilde{\sigma}^j_{lk}$ are the stresses due to dislocations $j \neq i$ and $\hat{\sigma}^i_{lk}$ are the image stresses acting on dislocation i gliding along the slip plane with unit normal m_l.

An obstacle present in the material pins approaching dislocations at its location. However if the shear stress τ exerted by the dislocation on that obstacle exceeds the obstacle strength τ_{obs}, or if the dislocation moves in the opposite direction, the dislocation breaks free and regains its mobility. Obstacles are placed on slip planes that contain at least one dislocation source.

If the path of a dislocation crosses the surface of the crystal at the contact or elsewhere, the dislocation escapes, leaving behind a crystallographic step of magnitude b at the surface. Since the step modifies the surface profile, it is added to the surface displacement $\mathbf{u}$ term in the gap functions (Eq. 2.4). The process of finding the contact solution remains unchanged.

Dislocation plasticity is inherently stochastic due to the statistical nature of the source and obstacle positions and the source strengths [1, 7–9]. For the analysis presented in this thesis, we perform six to eight realizations for each case to obtain the average response. Each realization differ in the location of the sources and obstacles in the body, and the source strengths, which are normally distributed.

The procedure to obtain the solution for contact between two bodies that can deform by dislocation plasticity is summarized in Fig. 2.4.

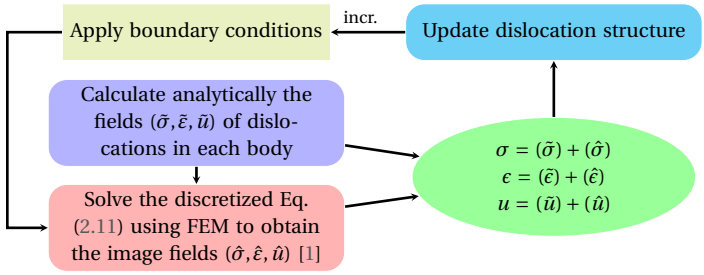

Figure 2.4: Steps to obtain the solution for two plastic bodies in contact at each time increment of the simulation.

REFERENCES

[1] K. Ng Wei Siang and L. Nicola, *Discrete dislocation plasticity analysis of contact between deformable bodies with simple geometry,* Model. Simul. Mater. Sci. **24**, 045008 (2016).

[2] P. Wriggers, *Computational Contact Mechanics 2002* (Wiley, 2002) p. 464.

[3] P. Papadopoulos and R. L. Taylor, *A mixed formulation for the finite element solution of contact problems,* Comput. Method Appl. Mech. Eng. **94**, 373 (1992).

[4] E. Van der Giessen and A. Needleman, *Discrete dislocation plasticity: a simple planar model,* Model. Simul. Mater. Sci. **3**, 689 (1995).

[5] L. P. Kubin, G. Canova, M. Condat, B. Devincre, V. Pontikis, and Y. Bréchet, *Dislocation microstructures and plastic flow: a 3D simulation,* Solid State Phenom. **23**, 455 (1992).

[6] J. R. Rice, *Tensile crack tip fields in elastic-ideally plastic crystals,* Mech. Mater. **6**, 317 (1987).

[7] H. Bei, S. H. Shim, G. M. Pharr, and E. P. George, *Effects of pre-strain on the compressive stress–strain response of* M*o-alloy single-crystal micropillars,* Acta Mater. **56**, 4762 (2008).

[8] C. Zhou, S. B. Biner, and R. LeSar, *Discrete dislocation dynamics simulations of plasticity at small scales,* Acta Mater. **58**, 1565 (2010).

[9] S. Yefimov, E. Van der Giessen, and I. Groma, *Bending of a single crystal: discrete dislocation and nonlocal crystal plasticity simulations,* Model. Simul. Mater. Sci. **12**, 1069 (2004).

3

DISCRETE DISLOCATION PLASTICITY ANALYSIS OF CONTACT BETWEEN DEFORMABLE BODIES OF SIMPLE GEOMETRIES

Every great and deep difficulty bears in itself its own solution.
It forces us to change our thinking in order to find it.

Niels Bohr

Parts of this chapter have been published in Model. Simul. Mater. Sci. **24**, 045008 (2016) [1].

3

Here, we will investigate the effect of contact conditions and size on the mechanical response of two bodies in contact using the formulation described in Chapter 2. While the formulation is general, the simulations presented in this chapter are only performed for the contact between a plastically deforming body with sinusoidal surface and a flat body that is either elastic or rigid.

Results show that the contact conditions, i.e. frictionless and full stick, affect the morphology of the contact as well as the contact pressure distribution. This is because dislocations can glide through the frictionless contact and fragment it, but do not penetrate a sticking contact. Average quantities like mean apparent contact pressure and total plastic slip are, instead, independent of contact conditions and of the details of the contact area.

A size dependence is observed in relation to the onset of plastic deformation, where surfaces with smaller wavelength and amplitude require a larger contact pressure to yield than self similar surfaces with larger wavelength. The size dependence is very pronounced when the flat body is rigid, but fades when the compliance of the flat body is large.

3.1. INTRODUCTION

UNDERSTANDING how surfaces deform upon contact is important in the process to realize or optimize many engineering applications, especially when the mechanism or the performance is altered by friction or wear [2–5]. Contact between surfaces is usually non-conformal, since a surface–even nominally flat–comprises many asperities, and only a fraction of the asperities support the load [2].

Considerable attention has been given to developing contact models that describe elastic-plastic deformation of the asperities in contact [6–11]. These analyses are based on continuum approaches, which assume the onset of plasticity to be size independent. Recent experiments on crystalline solids have however demonstrated that plasticity is size dependent at the (sub)-micron scale [12–17]. This implies that a micron sized asperity is harder to deform plastically than a self-similar larger asperity. Since the macroscopic behavior of rough surfaces is determined by the collective behavior of the asperities supporting the load, their size-dependent plastic response cannot be neglected.

Molecular dynamic simulations have been used to study nanoscale contacts [18, 19], but the technique is computationally too expensive to be used in analyzing contacts at a larger scale. At the micron scale, discrete dislocation plasticity [20] has been used to investigate contact deformation of a single or multiple asperities [21–25]. This method bridges the gap between the atomic scale and the continuum scale. Plasticity in the body is described by the collective motion of discrete edge dislocations, and by that the model contains the intrinsic length scale of plasticity: the Burgers vector.

With this method it is found that the plastic response of the body is independent of contact conditions [23]. However, the asperities in these studies are flattened through boundary conditions that mimic the effect of a rigid body. Dislocations are prevented from escaping the contact to preserve compatibility, for which they pile up beneath the contact. The question therefore arises on whether the contact pressure profiles are affected by this constraint.

The purpose of this work is to investigate how the results would differ when both bodies in contact are explicitly described. To this end a contact model is developed, and the formulation is as described in Chapter 2. We investigate how the contact conditions affect the plastic response of a metal single crystal with sinusoidal surface flattened by a rigid body. Finally, we explore how the size dependent plastic response of the sinusoidal surface [23] is affected by contact with a compliant platen.

3.2. CONTACT BETWEEN A PLATEN AND A BODY WITH SINUSOIDAL SURFACE

A two dimensional metal single crystal with a sinusoidal surface (body 1) is flattened by a platen (body 2) under plane strain conditions (see Fig. 3.1). Only body 1 can deform plastically by dislocations gliding along three sets of slip

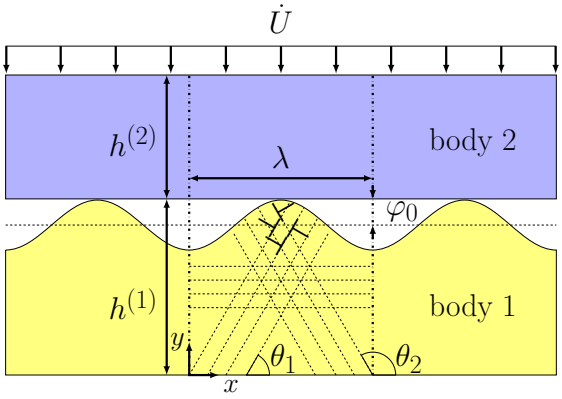

Figure 3.1: Two-dimensional model of a metal single crystal with sinusoidal surface (body 1) flattened by a platen (body 2). Body 1 can deform plastically by dislocation motion.

planes oriented at angles θ_i with respect to the x direction (see Chapter 2). The surface profile of body 1 is described by a sinusoid with wavelength λ and amplitude φ_0. Each wave of the sinusoid represents a surface asperity. The heights of body 1 and body 2 are $h^{(1)} - \varphi_0$ and $h^{(2)}$, respectively, where $\varphi_0 \ll h^{(1)}$. Taking advantage of periodicity, the analysis is performed only on a representative unit cell with wavelength λ.

3.2.1. BOUNDARY CONDITIONS

A uniform displacement is applied on the top surface of body 2,

$$u_y(x, h^{(1)} + h^{(2)}) = \int_0^t \dot{U}\,\mathrm{d}t, \tag{3.1}$$

where $\dot{U}$ is the displacement loading rate. Periodic boundary conditions are imposed on the lateral sides of the unit cell,

$$\mathbf{u}(0, y) = \mathbf{u}(\lambda, y). \tag{3.2}$$

The base of body 1 is fixed in y direction $u_y(x, 0) = 0$, and to prevent rigid body motion,

$$u_x\big(0, h^{(1)} + h^{(2)}\big) = u_x\big(0,0\big) = 0. \tag{3.3}$$

The contact is either frictionless or sticking.

3.2.2. MATERIAL PROPERTIES

Body 1 is taken to have the elastic properties of Al with Young's modulus $E = 70\,\text{MPa}$ and Poisson's ratio $\nu = 0.33$. The FCC crystal structure is modeled in two dimensions by considering three sets of parallel slip planes oriented at $\theta_1 = 0°, \theta_2 = 60°$ and $\theta_3 = 120°$ [26]. The spacing between slip planes with the same orientation is $200\,b$, where $b = 2.5\,\text{Å}$.

Dislocation sources and obstacles are distributed on the slip planes throughout the initially dislocation and stress free body 1. The dislocation source density ρ_{nuc} and obstacle density ρ_{obs} are $60\,\mu\text{m}^{-2}$ and $30\,\mu\text{m}^{-2}$, respectively. The source strength τ_{nuc} is distributed normally with a mean of 50 MPa and a standard deviation of 20 %, and the nucleation time t_{nuc} has a value of 10 ns. The obstacle strength τ_{obs} is assumed to have the value of 150 MPa. The drag coefficient D is assigned a value of $10^{-10}\,\text{MPa s}$.

3.3. RESULTS

3.3.1. EFFECT OF CONTACT CONDITIONS

In this section we investigate the influence of different contact conditions, frictionless and full stick, on the plastic response obtained from flattening body 1 with a rigid body 2. The rigid body has Young's modulus $E^{(2)} = 10^6\,E^{(1)}$; which is sufficiently small to prevent ill-conditioning of the finite element stiffness matrix. The asperity has wavelength $\lambda = 10\,\mu\text{m}$ and amplitude $\varphi_0 = 0.2\,\mu\text{m}$. The height of body 1 is $h^{(1)} = 15\,\mu\text{m}$, sufficiently large that plasticity is confined to the upper part of the crystal. Body 2 has height $h^{(2)} = 5\,\mu\text{m}$. Results are found to be independent of the height of body 2, as long as $h^{(2)}/\lambda > 0.2$.

The mean true contact pressure p_c is given as a function of the mean separation strain ε_g in Fig. 3.2a. The mean true contact pressure is calculated by dividing the contact force $F_c = \left(\int_{\gamma_c} \mathbf{t}\cdot n_y\,\mathrm{d}\Gamma\right)$ by the true contact area A_c. The mean separation strain ε_g is defined as $\varepsilon_g = (\Delta_0 - \Delta)/\Delta_0$, where Δ and Δ_0 denote the current and initial average separation distance, respectively (see Fig. 3.2b).

It is first verified that the elastic numerical solution (dashed line in Fig. 3.2a) agrees with the analytical solution, obtained as follows. From [27], the mean separation strain ε_g can be expressed as

$$\varepsilon_g = \sin^2\left(\frac{\pi A_c}{2\lambda}\right)\left[1 - \ln\left\{\sin^2\left(\frac{\pi A_c}{2\lambda}\right)\right\}\right], \tag{3.4}$$

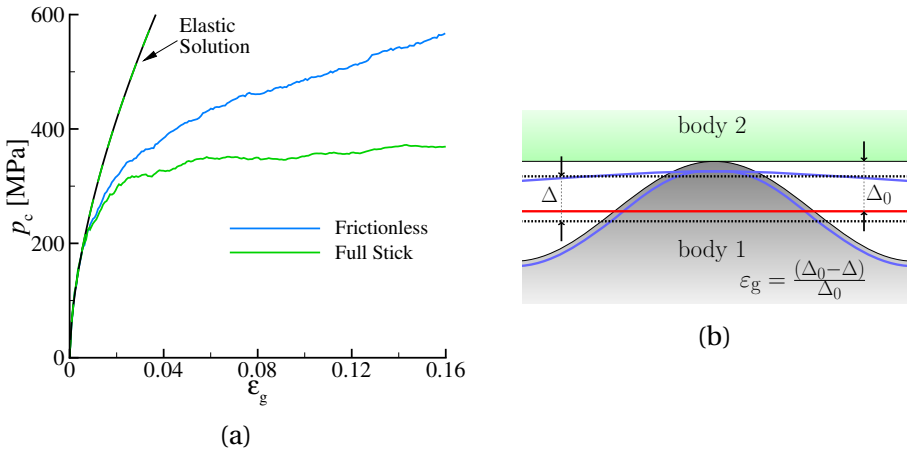

Figure 3.2: (a) Mean true contact pressure versus strain for both contact conditions. The dashed line represents the numerical elastic pressure. (b) Schematic representation of the strained surfaces. The dashed lines are the average profiles of the deformed surfaces.

where the contact area A_c is related to the contact force F_c [28] as

$$A_c = \frac{2\lambda}{\pi} \sin^{-1}\left(\sqrt{\frac{F_c}{\pi E' \varphi_0}}\right). \tag{3.5}$$

Here E' is the effective elastic modulus, given by $E' = [\left(1-(\nu^{(1)})^2\right)/E^{(1)} + \left(1-(\nu^{(2)})^2\right)/E^{(2)}]^{-1}$. The strain–pressure relation is obtained by substituting Eq. 3.5 into Eq. 3.4.

When plasticity is accounted for (solid lines in Fig. 3.2a), it is found that the true contact pressure–strain response depends on contact conditions. The curve for full stick contact shows practically no increase in pressure after yield, similarly to what is observed in a continuum study of flattening a frictionless sinusoidal surface by Gao *et al.* [29], while the pressure for frictionless contact increases with increasing strain. This is in contrast with the results for single body simulations obtained by Sun *et al.* [23], where the true pressure–displacement curves for frictionless and full stick contact overlapped with each other. In the following we will investigate how the contact conditions affect the plastic response of the body.

To estimate the amount of plastic activity in the crystal obtained with the different contact conditions, we present in Fig. 3.3a, b the plastic shear strain calculated at each point as the sum of the plastic shear strain along each slip direction. Comparing the plastic strain distribution for different contact conditions shows many local differences, but on average a similar response. A quantitative comparison is provided in Fig. 3.3c, where the ratio of the total slip for frictionless

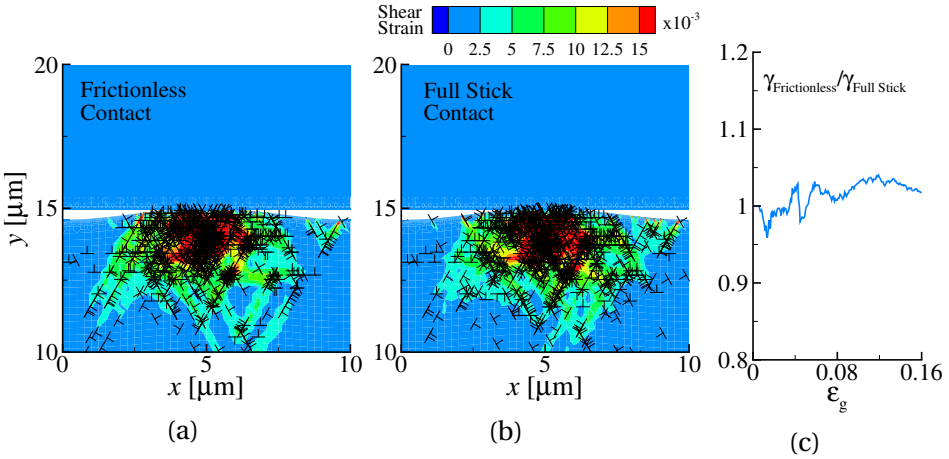

Figure 3.3: Plastic shear strain distribution for (a) frictionless and (b) full stick contacts for a particular realization. (c) Total slip in the bodies for the frictionless case compared to full stick.

contact $\gamma_{\text{Frictionless}}$ to full stick contact $\gamma_{\text{Full Stick}}$ is presented. The ratio is close to one, indicating that there is no sensible difference in the plastic activity. If

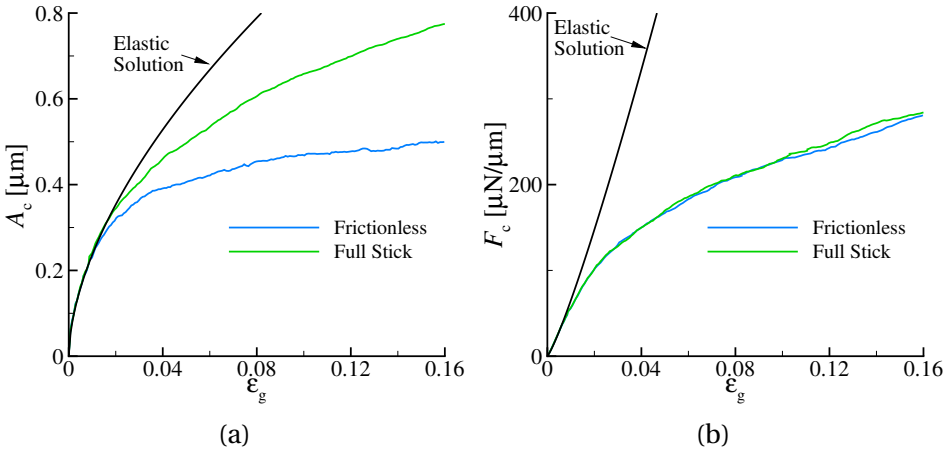

Figure 3.4: (a) True contact area A_c, and (b) contact force F_c as a function of the mean separation strain ε_g for both contact conditions.

this is the case, what causes the different contact pressure response? To reach a better understanding, the true contact area A_c and the contact force F_c are independently presented in Fig. 3.4a and Fig. 3.4b. It becomes now clear that the difference in true contact pressure is solely caused by a difference in true contact area, while the force necessary to press the bodies into contact is the same for frictionless and full stick contact.

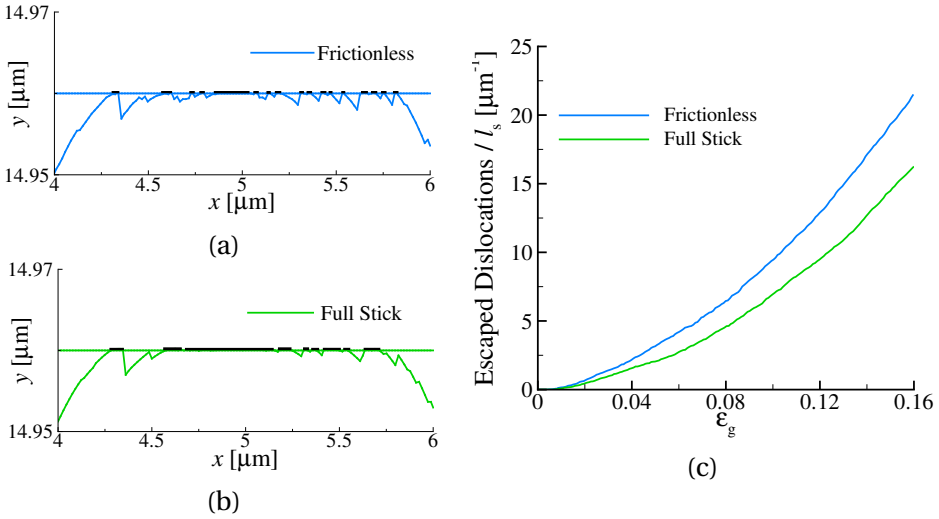

Figure 3.5: Surface profiles for (a) frictionless and (b) full stick conditions at $\varepsilon_g = 0.16$ of a particular realization. Contact is indicated by thick line segments. (c) Number of escaped dislocations per unit length l_s of the top surface of body 1.

The contact profiles are presented in Fig. 3.5a and b. The frictionless contact is made of many small patches, whereas the full stick contact has fewer and larger contact patches. Patchiness of the contacts is a consequence of the discreteness of dislocations and of dislocation slip planes. For a small flattening depth there is only a central continuous contact area, but as plasticity develops, new smaller contact areas form, in correspondence to dislocations gliding out of the free surface and causing small protrusions of the material. Similar profiles where observed also for single body simulations [23]. The difference with the single body simulations is that dislocations were not allowed to penetrate the contact, while in the two body problem they can, and they do when the contact is frictionless. Interestingly, the fact that more dislocations can escape the contact seems to have an impact only on the geometry of the contact area but not on the mechanical response of the bodies. This is because the number of dislocations that escape the contact is small (< 20 %) when compared to the number of dislocations that escape the rest of the top surface (traction free) of the sinusoidal body (see Fig. 3.5c).

Moreover, the apparent contact area (Fig. 3.6a), defined as the distance between the outermost contact edges, is the same for both contact conditions, so is the mean apparent contact pressure $p_a = F_c / A_a$ (Fig. 3.6b). This means that details of the true contact area do not affect the mean apparent contact pressure. Indeed loading the body through a continuous or a patchy contact, with

little spacing in between contact segments (here 40 nm on average) leads to a very similar elastic and plastic response. Since the average spacing of the sources (~ 130 nm) is much larger than the gaps between the patches, the likelihood of finding a source near the gaps is small, and the resulting plastic slip is the same as if the contact were continuous (Fig. 3.3c).

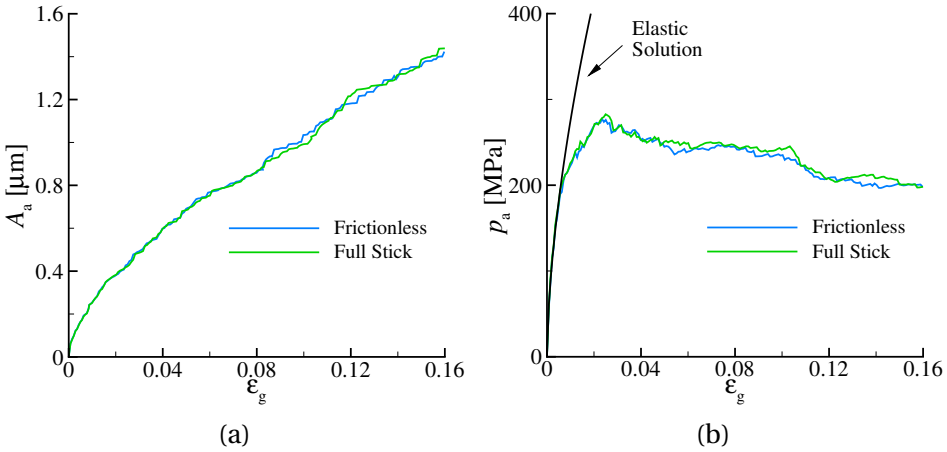

Figure 3.6: (a) Apparent contact area A_a and (b) apparent contact pressure p_a for frictionless and full stick conditions.

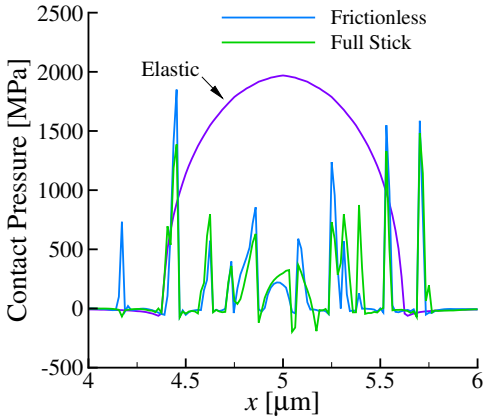

Figure 3.7: Contact pressure distribution, $-p_y(x)$, at $\varepsilon_g = 0.16$

Nevertheless, the local contact pressure distribution $p_y(x) = -\mathbf{t}(x) \cdot n_y$, presented in Fig. 3.7 is highly dependent on the patchy nature of the contact area and therefore on contact conditions. The pressure is characterized by high peaks with values up to two orders of magnitudes larger than the macroscopic tensile

yield strength of Al. Frictionless contact is the most patchy and has therefore the highest peaks. The large pressure peaks across the contact of the asperity, which are a result of the discreteness of dislocations and slip planes, are not observed in continuum contact studies. For instance, a local continuum plasticity study on the flattening of sinusoidal surfaces [29] shows that the contact pressure is continuous, since the contact area is also continuous. The two studies do not only differ in terms of pressure profiles. The mean contact pressure obtained at small flattening depth using discrete dislocation plasticity is larger (almost double) than what is found in the continuum model.

3.3.2. CONTACT BETWEEN AN ELASTIC AND A PLASTICALLY DEFORMING BODY

In this section the platen, body 2, is taken to be elastic and to have the same elastic properties as body 1. The results are compared with the results in Sec. 3.3.1, where body 2 is rigid. The effective elastic modulus is $E' = 39.3\,\text{GPa}$ when body 2 is rigid and $E' = 78.5\,\text{GPa}$ when it is elastic. Given that in the previous section the plastic response of the crystal was found to be independent of contact conditions, we choose here to study only one of the two conditions, i.e. frictionless, and present the response in terms of apparent contact pressure. As expected, the

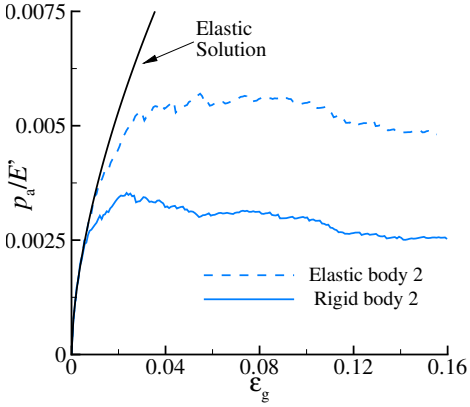

Figure 3.8: Normalized mean apparent contact pressure p_a for contact with an elastic and a rigid Body 2.

normalized mean apparent contact pressure p_a/E' presented in Fig. 3.8 deviates from the elastic solution at a larger strain ε_g when body 2 is elastic. However, at strains $\varepsilon_g > 0.04$, the curves have approximately the same shape, independent of the properties of body 2. Figure 3.9 shows the shear stress resolved in the direction of the slip planes with $\phi = 60°$, $\tau_{60°}$, and the dislocation distribution for both cases at strain $\varepsilon_g = 0.04$. A larger dislocation density is found when body 2

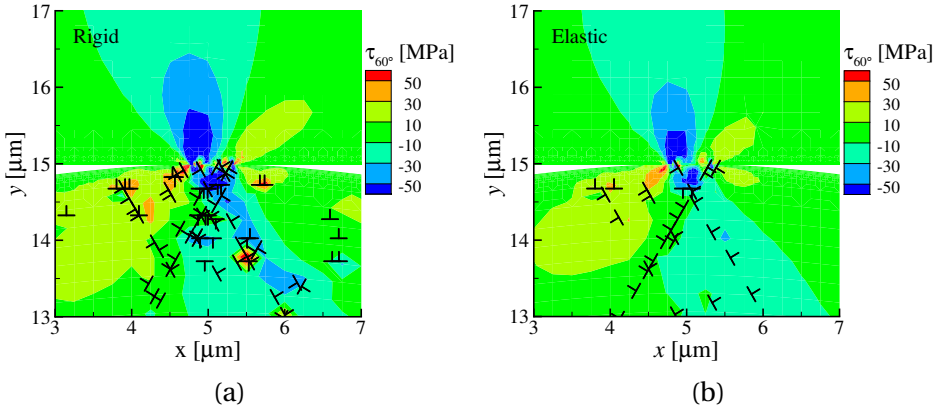

Figure 3.9: The resolved shear stress τ_{60° for contact with (a) a rigid and (b) an elastic Body 2 at strain $\varepsilon_g = 0.04$.

is rigid, given that the rigid body has induced a larger deformation on body 1.

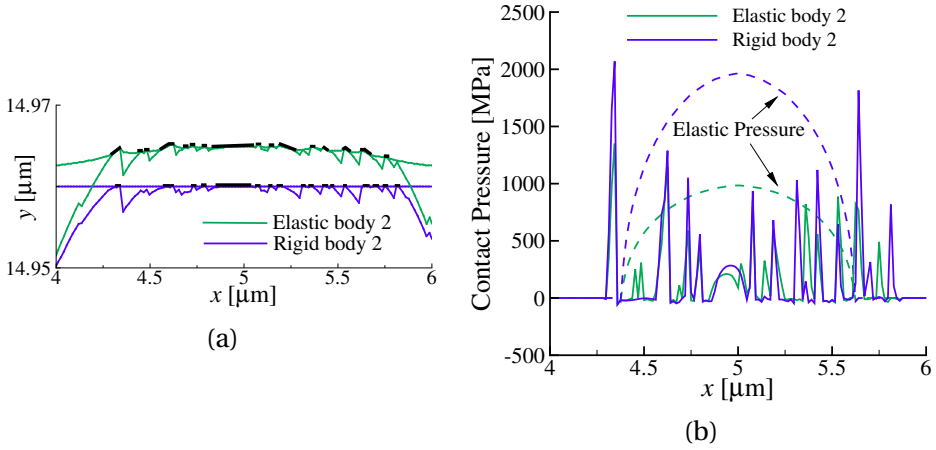

Figure 3.10: (a) Surface profile at strain $\varepsilon_g = 0.16$ for contact with an elastic and a rigid Body 2. Contact is indicated by thick line segments. (b) The corresponding contact pressure.

The contact profile for both cases is shown in Fig. 3.10a. The surface of the elastic body 2 conforms to the surface of body 1, and the contact height is larger. The size of the contact patches are also, on average, larger when body 2 is elastic. As a result, the pressure distribution at the contact, given in Fig. 3.10b when body 2 is elastic, is characterized by smaller peaks compared with the case in which body 2 is rigid.

3.3.3. SIZE DEPENDENT RESPONSE OF SCALED ASPERITIES

Previous discrete dislocation plasticity simulations [23] have demonstrated that the plastic behavior of micron-sized asperities flattened by a rigid platen is size dependent. Here we investigate if this size effect is still significant when the asperities are flattened by an elastic platen. To this end, asperities having constant aspect ratio, $\lambda/\varphi_0 = 50$, and amplitudes $\varphi_0 = 0.2, 0.1$, and $0.05\,\mu$m are flattened by an elastic and a rigid platen.

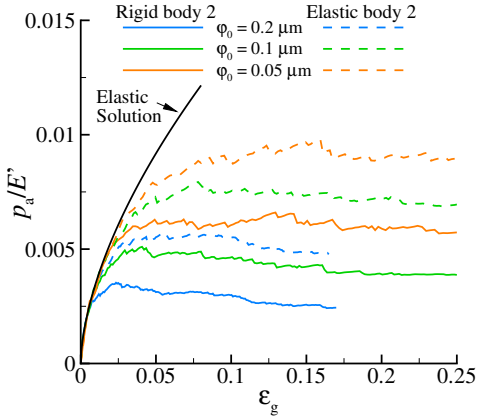

Figure 3.11: The normalized apparent contact pressure p_a/E' for scaled asperities.

Figure 3.11 shows the normalized contact pressure as a function of strain for scaled asperities. In terms of the onset of plasticity, a size effect is found for both cases: as the asperity size decreases, the normalized pressure p_a/E' deviates from the elastic solution at a larger strain. After the onset of plasticity differences in the shape of the curves are no longer appreciable.

The reason for the size effect is that the size of the critical stress zone at a given strain scales with asperity size, while the average source spacing is a constant, $\sqrt{1/\rho_{\text{nuc}}} = 0.130\,\mu$m. Plasticity in the smaller asperities is therefore source limited. For instance at strain $\varepsilon_g = 0.03$ when body 2 is elastic, dislocation nucleation already occurs for the larger asperity (Fig. 3.12a), whereas the deformation is still elastic for the smaller asperity (Fig. 3.12b). However, as the size of the stress zone increases with load, deformation becomes no longer source limited as more sources lie in the critical zone, leading to approximately the same rate of plastic relaxation of the stresses for all asperity sizes.

To evaluate how the size effect depends on the elastic properties of the flattening body, scaled asperities with aspect ratio $\lambda/\varphi_0 = 50$ and volumes $V_{\text{asp}} = \lambda\varphi_0 = 0.125, 0.245, 5.0, 1.0, 2.0, 4.0$ and $8.0\,\mu$m^2 are here flattened by a rigid, and by two elastic bodies with different compliance, giving $E' = 39.3$ GPa and $E' =$

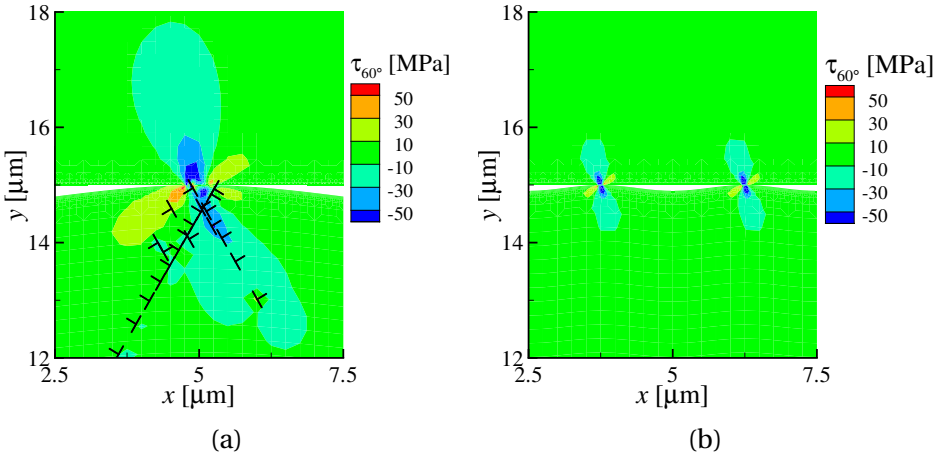

Figure 3.12: Resolved shear stress $\tau_{60°}$ for asperity amplitude (a) $\varphi_0 = 0.2\,\mu$m ($\lambda = 10\,\mu$m), and (b) $\varphi_0 = 0.05\,\mu$m ($\lambda = 2.5\,\mu$m) at strain $\varepsilon_g = 0.03$. Body 2 is elastic.

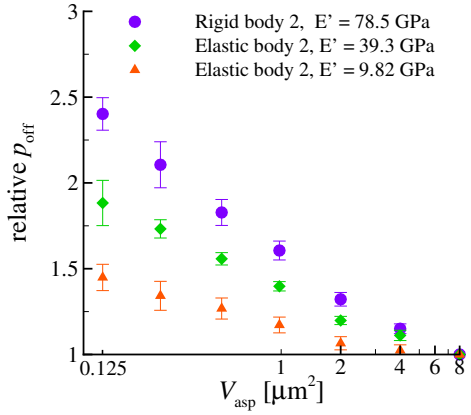

Figure 3.13: Relative offset pressure as function of asperity volume V_{asp}. Each vertical bar is the standard deviation of six realizations.

9.82 GPa. The apparent pressure required to reach a 2 % offset strain p_{off} is calculated for all asperities. We present in Fig. 3.13 all results in terms of the relative offset pressure p_{off}, defined as the offset pressure of each asperity with respect to the largest asperity ($V_{asp} = 8.0\,\mu$m^2). The contact response of the largest asperity approaches the continuum limit. The relative offset pressure increases with decreasing size and, as expected, the increase is smaller for a smaller elastic modulus $E^{(2)}$. This indicates that the size effect is smaller when body 1 is deformed by a more compliant body 2. Obviously, in the limit $E' \to 0$, no size effect will be observed since deformation is elastic for both bodies.

3.4. CONCLUSIONS

A contact model is developed to simulate the mechanical response of bodies that can both deform by dislocation plasticity. Despite the model is general, we here confine our attention to two dimensional simulations of the contact between a body with sinusoidal surface that can plastically deform and a platen that can either deform elastically or behave rigidly.

Flattening by means of a rigid body is performed to understand the effect of limiting contact conditions; the surface is either full stick or frictionless. Results show that the geometry of the true contact area, hence the contact pressure profiles depend on contact conditions: frictionless contacts are more patchy than full stick contacts and therefore are characterized by larger pressure peaks. The difference in contact area profiles is caused by the fact that dislocations can glide through the contact regions in the case of frictionless contacts. This was not possible in previously performed discrete dislocation plasticity simulations of contact, where the effect of the rigid platen was modeled by prescribing boundary conditions on the deformable body. However, the effect of contact conditions on the apparent contact area, apparent contact pressure and plastic slip in the crystal is found to be negligible. The exact morphology of the true contact area affects the local pressure but not its mean, or the overall plastic behavior. This is attributed to the fact that the spacing between contact segments is very small, smaller than the average dislocation source spacing.

The simulations also show a size dependent plastic response with smaller asperities being harder to deform than larger asperities. The size effect becomes less pronounced when the compliance of the flattening body increases. The size dependence involves only the onset of plasticity and is caused by source limitation. For larger strains, with the increase of the loaded area, the source limitation disappears and the mean contact pressure is approximately constant with increasing strain.

REFERENCES

[1] K. Ng Wei Siang and L. Nicola, *Discrete dislocation plasticity analysis of contact between deformable bodies with simple geometry,* Model. Simul. Mater. Sci. **24**, 045008 (2016).

[2] F. P. Bowden and D. Tabor, *The friction and lubrication of solids*, Vol. 1 (Oxford: Claredon, 1950).

[3] A. Ronen, I. Etsion, and Y. Kligerman, *Friction-reducing surface-texturing in reciprocating automotive components,* Tribol. Trans. **44**, 359 (2001).

[4] A. Khurshudov and R. J. Waltman, *Tribology challenges of modern magnetic hard disk drives,* Wear **251**, 1124 (2001).

[5] C. R. Liu and Y. B. Guo, *Finite element analysis of the effect of sequential cuts and tool–chip friction on residual stresses in a machined layer,* Int J. Mech. Sci. **42**, 1069 (2000).

[6] A. Majumdar and B. Bhushan, *Fractal model of elastic-plastic contact between rough surfaces,* J. Tribol. T. ASME. **113**, 1 (1991).

[7] W. R. Chang, I. Etsion, and D. B. Bogy, *An elastic-plastic model for the contact of rough surfaces,* J. Tribol. T. ASME. **109**, 257 (1987).

[8] L. Kogut and I. Etsion, *A finite element based elastic-plastic model for the contact of rough surfaces,* Tribol. Trans. **46**, 383 (2003).

[9] Y. W. Zhao, D. M. Maietta, and L. Chang, *An asperity microcontact model incorporating the transition from elastic deformation to fully plastic flow,* Tribol. Trans. **122**, 86 (2000).

[10] D. G. Evseev, B. M. Medvedev, and G. G. Grigoriyan, *Modification of the elastic-plastic model for the contact of rough surfaces,* Wear **150**, 79 (1991).

[11] Z. Song and K. Komvopoulos, *Elastic–plastic spherical indentation: Deformation regimes, evolution of plasticity, and hardening effect,* Mech. Mater. **61**, 91 (2013).

[12] Q. Ma and D. R. Clarke, *Size dependent hardness of silver single crystals,* J. Mater. Res. **10**, 853 (1995).

[13] M. D. Uchic, D. M. Dimiduk, J. N. Florando, and W. D. Nix, *Sample dimensions influence strength and crystal plasticity,* Science **305**, 986 (2004).

[14] J. R. Greer, W. C. Oliver, and W. D. Nix, *Size dependence of mechanical properties of gold at the micron scale in the absence of strain gradients,* Acta Mater. **53**, 1821 (2005).

[15] J. R. Greer and W. D. Nix, *Size dependence of mechanical properties of gold at the sub-micron scale,* Appl. Phys. A **80**, 1625 (2005).

[16] L. Nicola, Y. Xiang, J. J. Vlassak, E. Van der Giessen, and A. Needleman, *Plastic deformation of freestanding thin films: experiments and modeling,* J. Mech. Phys. Solids **54**, 2089 (2006).

[17] D. Kiener, W. Grosinger, G. Dehm, and R. Pippan, *A further step towards an understanding of size-dependent crystal plasticity: In situ tension experiments of miniaturized single-crystal copper samples,* Acta Mater. **56**, 580 (2008).

[18] B. Luan and M. O. Robbins, *The breakdown of continuum models for mechanical contacts,* Nature **435**, 929 (2005).

[19] Y. Mo and I. Szlufarska, *Roughness picture of friction in dry nanoscale contacts,* Phys. Rev. B **81**, 035405 (2010).

[20] E. Van der Giessen and A. Needleman, *Discrete dislocation plasticity: a simple planar model,* Model. Simul. Mater. Sci. **3**, 689 (1995).

[21] L. Nicola, A. F. Bower, K. S. Kim, A. Needleman, and E. Van der Giessen, *Multi-asperity contact: a comparison between discrete dislocation and crystal plasticity predictions,* Philos. Mag. **88**, 3713 (2008).

[22] X. Yin and K. Komvopoulos, *A discrete dislocation plasticity analysis of a single-crystal semi-infinite medium indented by a rigid surface exhibiting multi-scale roughness,* Philos. Mag. **92**, 2984 (2012).

[23] F. Sun, E. Van der Giessen, and L. Nicola, *Plastic flattening of a sinusoidal metal surface: A discrete dislocation plasticity study,* Wear **296**, 672 (2012).

[24] Y. Zhang, Y. F. Gao, and L. Nicola, *Lattice rotation caused by wedge indentation of a single crystal: Dislocation dynamics compared to crystal plasticity simulations,* J. Mech. Phys. Solids **68**, 267 (2014).

[25] R. J. Dikken, E. Van der Giessen, and L. Nicola, *Plastic shear response of a single asperity: a discrete dislocation plasticity analysis,* Philos. Mag. **95**, 3845 (2015).

[26] J. R. Rice, *Tensile crack tip fields in elastic-ideally plastic crystals,* Mech. Mater. **6**, 317 (1987).

[27] Y. A. Kuznetsov, *Effect of fluid lubricant on the contact characteristics of rough elastic bodies in compression,* Wear **102**, 177 (1985).

[28] H. M. Westergaard, *Bearing pressures and cracks,* J. Appl. Mech. **6**, 49 (1939).

[29] Y. F. Gao, A. F. Bower, K. S. Kim, L. Lev, and Y. T. Cheng, *The behavior of an elastic-perfectly plastic sinusoidal surface under contact loading,* Wear **261**, 145 (2006).

4

CONTACT BETWEEN TWO PLASTICALLY DEFORMABLE CRYSTALS

If we knew what it was we were doing,
it would not be called research, would it?

Albert Einstein

Parts of this chapter are in an article submitted to Philos. Mag. [1].

4

It is customary to simplify the analysis of contact between two elastically deformable bodies by treating an equivalent problem where only one body is deformable and the other is rigid. This is possible provided that the gap geometry and the effective elastic modulus of the bodies in the simplified problem are the same as in the original problem. However, the question arises on whether – and to which extent – the simplification is still valid even when (size-dependent) plasticity occurs.

Studies using discrete dislocation plasticity have also, so far, addressed simple contact problems where only one body can deform plastically. Here, we extend the analysis to two bodies in contact that can both deform by dislocation plasticity and investigate under which conditions the response agrees with that of an equivalent simplified problem.

The bodies in contact are metal single crystals with sinusoidal and flat surface. The crystals are taken to have properties of Al or Cu. The size-dependent plastic response of Al against Al is found to be qualitatively similar to that of Cu against Cu. Also, it is found that the response of two plastically deformable bodies in contact can be simplified to an equivalent problem where one body is rigid and the other can deform plastically. Necessary conditions are that the source strength in the simplified problem is that of the softest material in the original problem, and that the source density is equal to the sum of the source densities contained in the two deformable crystals.

4.1. INTRODUCTION

FRICTION and wear of surfaces play a paramount role in the performance of many engineering machines, especially of micron and smaller sized devices in which surface effects become dominant [2–5]. These dissipative phenomena generally reduce the reliability and robustness of micron-sized devices such as actuators or motors as they result in wear of contact junctions [6, 7]. Clearly, to control and enhance the reliability and performance of these miniaturized devices, the behavior of the deforming bodies in contact must be understood.

Recently discrete dislocation plasticity simulations have been carried out to analyze the contact behavior of micrometer sized metal crystals [8–11]. The choice of this method is linked to the scale considered, which is too computationally expensive to be studied using molecular dynamics [12, 13]. Local and nonlocal continuum plasticity models [14–16] are also not suitable as they do not capture the effects caused by the discreteness of plastic carriers [17], e.g. source limitation effects [18–20], patchy contact areas and highly localized contact pressure peaks [21]. Discrete dislocation plasticity accounts for these effects as it considers the nucleation and glide of individual dislocations [9, 11].

So far the mechanical behavior of contact between micrometer sized sinusoidal asperities, or protrusions of a surface, and a rigid [9] or an elastic platen [11] has been investigated using discrete dislocation plasticity. A plasticity size effect is observed, for which smaller asperities are harder to deform. The size effect decreases with increasing compliance of the platen [11]. Here, we extend the analysis to two bodies that can deform by dislocation plasticity. Simulations of contact between a body with micron-sized sinusoidal asperities and a platen are performed. The crystals have properties of Cu or Al. Rather unexpectedly the plastic size dependence found is approximately the same.

To model the contact behavior of two deformable bodies, several local continuum contact studies simplify the problem to treat either a body having asperities in contact with a rigid flat body [22–27], or a rigid rough body in contact with a flat body [28–30]. This is because the elastic mechanical response of the two systems is the same, provided that the gap geometry and the effective elastic modulus of the bodies are the same (see e.g. [28]). The stresses in the region directly above and below the contact are also approximately the same, and they are a function of the effective elastic modulus, and not the elastic properties of each body. Thanks to this equivalence only the deformation of one body has to be considered since contact with the rigid body can be mimicked through boundary conditions. However in these studies, the deformable body also undergoes plastic deformation, and the validity of this simplification has been questioned [25, 27, 31, 32]. Can we use the simplified problem to predict

the behavior of contact between two micrometer sized crystals?

To answer this question we need to find out if the plastic properties of two crystals can be mapped to the plastic properties of one body in contact with a rigid body. We begin first by understanding the effect of surface geometry on the plastic response. To this end we investigate whether flattening of a sinusoidal body by a rigid platen is equivalent to the indentation of a platen by a rigid sinusoidal body, even when plasticity occurs. Next, we study how the contact response is affected when changing plastic properties of the bodies; i.e. dislocation source density and their critical strength as well as obstacle density and strength. Finally we determine which criteria should be met by an equivalent simplified system, in order to represent contact deformation between two plastically deforming metal crystals.

4.2. CONTACT BETWEEN A PLATEN AND A BODY WITH A SINUSOIDAL SURFACE

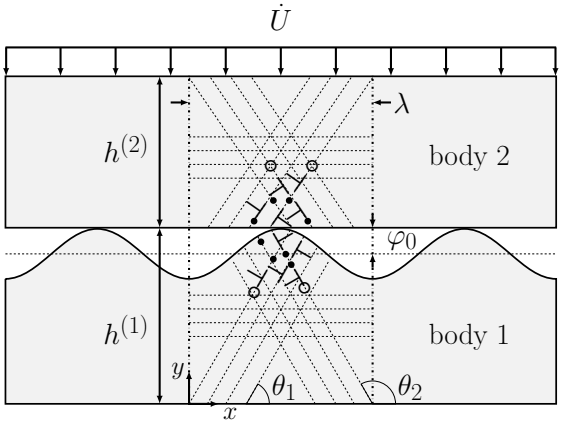

Figure 4.1: Two-dimensional model of a single crystal with sinusoidal surface in contact with a flat single crystal. Sources (·) and obstacles (∘) are homogeneously distributed in the bodies.

FIGURE 4.1 illustrates the problem of contact between two metal crystals under plane strain conditions. Both crystals deform plastically by edge dislocations gliding along three sets of slip planes oriented at an angle θ_i with the x direction. The surface profile of body 1, the bottom crystal, is described by a sinusoid with wavelength λ and amplitude φ_0. Each wave of the sinusoid represents an asperity. Body 2, the top crystal, has a flat surface profile. The heights of body 1 and body 2 are $h^{(1)}-\varphi_0$ and $h^{(2)}$ respectively, where $\varphi_0 \ll h^{(1)}$. Heights $h^{(1)}$ and $h^{(2)}$ are both 15 μm, sufficiently large that dislocation activity in the crystal

is confined to the region directly beneath the contact. This is to avoid that dislocations interact with the bottom of the crystal. The analysis is performed on a unit cell with a periodicity λ, where periodic boundary conditions are imposed, $\mathbf{u}(0,y) = \mathbf{u}(\lambda,y)$.

To establish contact a uniform displacement is applied on the top surface of body 2,

$$u_{\mathrm{y}}(x, h^{(1)} + h^{(2)}) = \int_0^t \dot{U}\,\mathrm{d}t, \tag{4.1}$$

where $\dot{U}$ is the displacement loading rate. The base of body 1 is fixed in the y direction $u_{\mathrm{y}}(x,0) = 0$, and to prevent rigid body translation, $u_{\mathrm{x}}(0, h^{(1)} + h^{(2)}) = u_{\mathrm{x}}(0,0) = 0$.

4.3. RESULTS

4.3.1. SIZE DEPENDENT RESPONSE OF TWO PLASTICALLY DEFORMING BODIES

Discrete dislocation plasticity simulations demonstrate that the plastic behavior of micron-sized scaled asperities flattened by a rigid [9] or an elastic platen [11] is size dependent. Here, we investigate if the size dependent plastic response is significant when both the asperity and platen can deform plastically. We simulate contact between crystals that have properties, both either resembling Al or Cu, as given in Table 4.1.

Material Properties	**Al**	**Cu**
Poisson ratio ν	0.33	0.35
Elastic modulus E	70 GPa	140 GPa
Burgers vector b	0.25 nm	0.23 nm
Drag coefficient D	10^{-10} MPas	1.5×10^{-11} MPas
Source strength τ_{nuc}	50 MPa $\pm$ 20 %	140 MPa $\pm$ 20 %
Obstacle strength τ_{obs}	150 MPa	150 MPa
Source density ρ_{nuc}	30 μm^{-2}	30 μm^{-2}
Obstacle density ρ_{obs}	15 μm^{-2}	15 μm^{-2}
Nucleation time t_{nuc}	10 ns	10 ns

Table 4.1: List of material properties used in the simulations to characterize single crystals Al and Cu.

The Al crystals have an effective elastic modulus $E' = [(1-(\nu^{(1)})^2)/E^{(1)} + (1-(\nu^{(2)})^2)/E^{(2)}]^{-1} = 39.3$ GPa, and the Cu crystals have $E' = 79.8$ GPa. The strength

of the dislocation sources of each material are obtained by performing a uniform compression simulation on each material and fitting the parameters to give the experimental material yield strength, while the source density is kept constant.

The asperities have constant aspect ratio, $\varphi_0/\lambda = 0.05$, and $\varphi_0 = 0.5, 0.25$, and $0.125\,\mu$m. The mean apparent pressure $p_a = \int_{\Gamma\in\gamma_c} (\mathbf{t}\cdot\mathbf{n}_y\,d\Gamma/A_a)$ is considered, where A_a is the apparent area calculated as the distance between the outermost contact edges, and $\mathbf{n}_y$ is the unit y vector. The normalized pressure p_a/E' is pre-

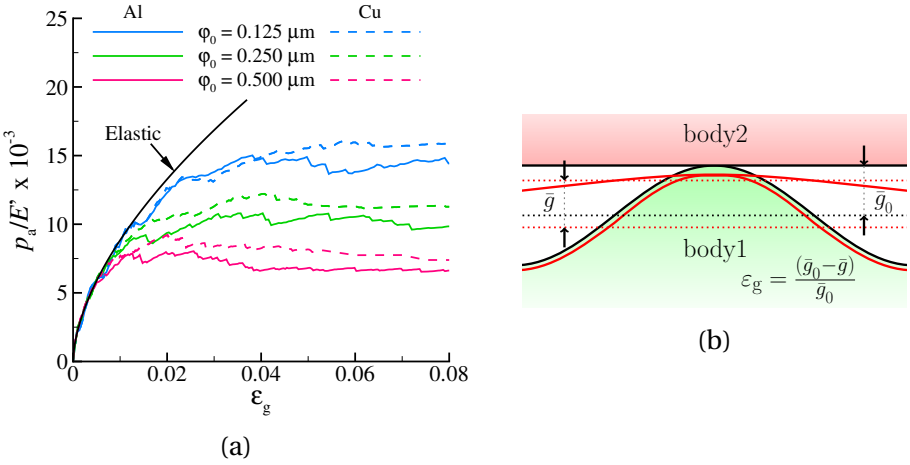

Figure 4.2: (a) The normalized apparent pressure, p_a/E', for scaled asperities in contact with a platen, both bodies having properties resembling Al, or Cu. (b) Schematics to illustrate the definition of strain, ε_g.

sented in Fig. 4.2a as a function of strain ε_g, defined as $(\bar{g}-\bar{g}_0)/\bar{g}_0$. Here $\bar{g}$ and $\bar{g}_0$ are the current and initial average gap (Fig. 4.2b). Elastically, p_a/E' for both cases overlap [11].

For both Al crystals and Cu crystals in contact the normalized apparent pressure at the onset of plasticity is larger for the smaller asperity, indicating a size effect. At larger strains, differences are no longer appreciable. This is because plasticity is source limited only for very small contact sizes, when the critical stress region (where $\tau > \bar{\tau}_{nuc}$) is small and therefore deprived of dislocation sources. A similar size dependence is found when flattening scaled micron-sized asperities using an elastic platen [11].

Comparing the normalized pressure for contact between Al crystals and between Cu crystals for a particular asperity size, we can observe that deviation from the elastic solution occurs at approximately the same strain, even though the effective elastic modulus of the Cu crystals is larger than for the Al crystals, and therefore leads to larger elastic stress levels in the bodies at a given strain.

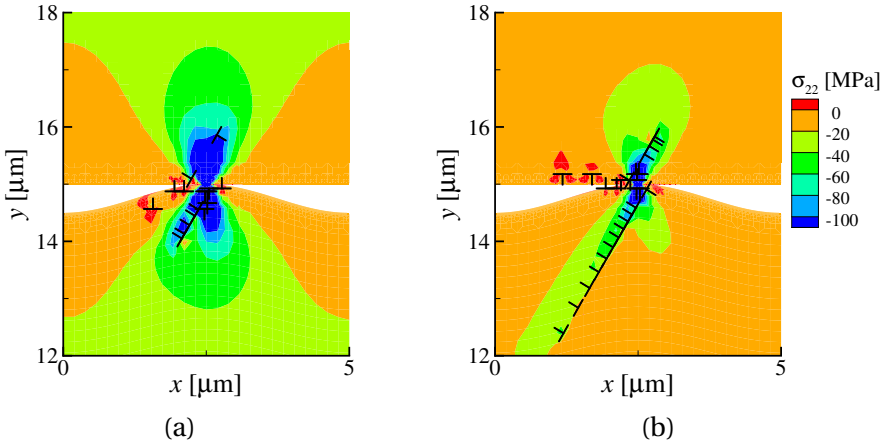

Figure 4.3: (a) Stress σ_{22} and dislocation distributions for contact between bodies with (a) Cu, and (b) Al properties at strain offset of 1 % for $\varphi_0 = 0.25\,\mu$m.

This is because the nucleation strength τ_{nuc} for Cu is also larger than for Al. For instance at strain offset of 1 % when $\varphi_0 = 0.25\,\mu$m, the dislocation density for Cu (Fig. 4.3a) is smaller than for Al (Fig. 4.3b), even if the stresses are larger. This leads to the approximately same normalized pressure response for Al crystals in contact and Cu crystals in contact. The normalized pressure for other FCC metal single crystals in contact is expected not to deviate greatly from the response observed here, since a pure FCC metal crystal with a larger E generally has on average stronger sources.

4.3.2. EFFECT OF SURFACE GEOMETRY

Here, we investigate how the plastic behavior of the bodies in contact depends on surface geometry. To this end we consider two limit cases: plasticity occurring only in the body with a sinusoidal surface, and plasticity occurring only in the platen. The other body in contact is rigid, and has a Young's modulus $E^{(2)} = 10^6\,E^{(1)}$; $E^{(2)}$ is sufficiently small to prevent ill-conditioning of the finite element stiffness matrix. The plastically deformable body in each case has the material properties of Al. The asperity has $\varphi_0 = 0.4\,\mu$m and $\lambda = 5.0\,\mu$m.

Figure 4.4a shows that the mean apparent pressure is larger when the platen is plastic. This shows that the plastic contact response does not only depend on the gap geometry and effective elastic modulus, but also on the surface geometry. As to be expected, the difference in contact pressure increases with increasing the amplitude of the sinusoid (Fig. 4.4b), but is however, given the large scatter of the results, only appreciable for $\varphi_0 > 0.25\,\mu$m.

Given that the elastic stress distribution in the platen is very similar to that in

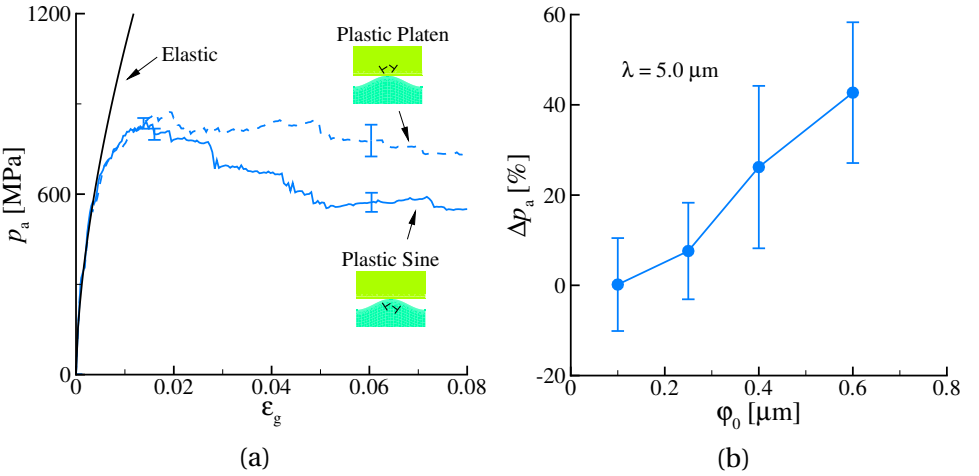

Figure 4.4: (a) The apparent pressure for contact between a rigid platen against a plastic body with a sinusoidal surface and a plastic platen against a rigid body with a sinusoidal surface for $\varphi_0 = 0.4\,\mu$m. Each vertical bar is the standard deviation obtained from eight simulations. (b) Pressure difference for the two cases taken at $\varepsilon_g = 0.06$ for various gap geometries.

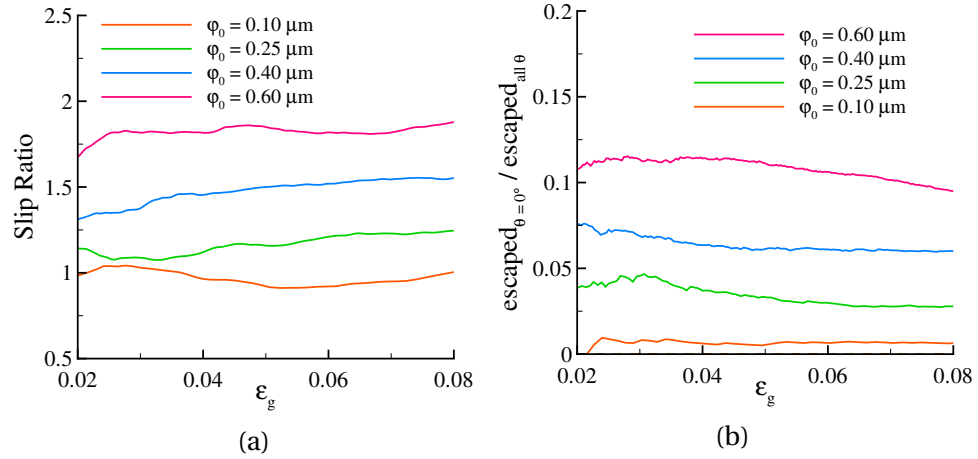

Figure 4.5: (a) Ratio of slip: slip obtained when the body with sinusoidal surface is plastic to slip when the platen is plastic for different φ_0, and (b) ratio of number of escaped dislocations from 0° slip planes to the total number of dislocations for the plastically deformed asperity for $\varepsilon_g > 2\,\%$.

the sinusoidal body for all amplitudes considered, it is far from self-evident what causes the different plastic response. The amount of slip caused by dislocations gliding in the sinusoidal body is larger than that obtained by dislocations gliding in the flat body, as testified by the slip ratio in Fig. 4.5a. The slip is obtained by integrating the total plastic shear strain of the three slip plane systems over the

volume of the body. As φ_0 increases from 0.1 μm to 0.6 μm, the slip increases when the body with a sinusoidal surface is plastic. What causes this increase?

We know that dislocations nucleated on the slip planes normal to the loading direction, with $\theta_1 = 0°$, can escape the sinusoidal surface. When this happens, more nucleations and dislocation glide can occur, which results in larger slip. Increasing the amplitude of the sinusoid, φ_0, increases the number of slip planes with $\theta_1 = 0°$, and hence the number of escaped dislocations from these slip planes in the plastically deformable asperity (Fig. 4.5b). This hypothesis is confirmed by performing simulations with only symmetric double slip (60° and 120° slip planes) for $\varphi_0 = 0.40\,\mu$m and 0.60 μm. Indeed as seen in Fig. 4.6a, p_a is statistically the same for both cases, when plasticity occurs in the body with a sinusoidal surface and when plasticity occurs in the platen.

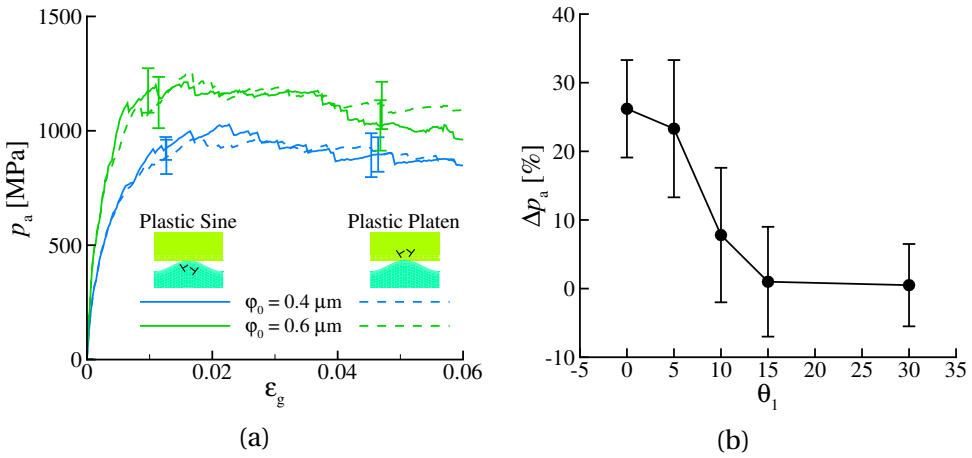

Figure 4.6: (a) Mean apparent pressure for $\varphi_0 = 0.4\,\mu$m and $\varphi_0 = 0.6\,\mu$m for symmetric double slip. (b) Percentage difference of the pressure between the cases (plastic platen or plastic sine) at strain $\varepsilon_g = 0.06$ when $\varphi_0 = 0.4\,\mu$m for different θ_1. Each vertical bar is the standard deviation obtained from eight simulations.

We also do not expect a difference between the cases (plastic platen or plastic sine) when none of the three active slip planes is oriented at 0°. Figure 4.6b shows the percentage pressure difference between the cases for $\theta_1 = 5°, 10°, 15°$ and 30° when $\varphi_0 = 0.4\,\mu$m at $\varepsilon_g = 0.06$. Indeed as θ_1 increases, Δp_a decreases until no appreciable difference is observed at $\theta_1 > 5°$.

Since the likelihood of slip planes being oriented at angles near 0° is small, and that asperities have $\varphi_0 \lll \lambda$ for most real surfaces [33], the number of slip planes that begin and end in the asperity is small. This means that the plastic response of flattening a body with sinusoidal surface with a rigid flat body can be considered the same as indenting a flat body with a rigid body with sinusoidal

surface.

4.3.3. EFFECT OF SOURCE DENSITY

Here, we investigate how the response is affected by changing the dislocation source density. To this end we take the liberty to change the source density ρ_{nuc} in each body while keeping the other material properties unchanged. The total source density $\rho_{\text{nuc}}^{(1)} + \rho_{\text{nuc}}^{(2)}$, is kept constant. Three different source densities in each body are considered: $\rho_{\text{nuc}}^{(1)} = \rho_{\text{nuc}}^{(2)} = 30\,\mu\text{m}^{-2}$; $\rho_{\text{nuc}}^{(1)} = 45\,\mu\text{m}^{-2}, \rho_{\text{nuc}}^{(2)} = 15\,\mu\text{m}^{-2}$; and $\rho_{\text{nuc}}^{(1)} = 60\,\mu\text{m}^{-2}, \rho_{\text{nuc}}^{(2)} = 0\,\mu\text{m}^{-2}$. The asperity has $\varphi_0 = 0.25\,\mu\text{m}$ so that the asperity is not too protruding, and the first set of slip planes is oriented at $\theta_1 = 15°$, to eliminate any difference in the plastic response resulting from the orientation of the slip planes (see Sec. 4.3.2).

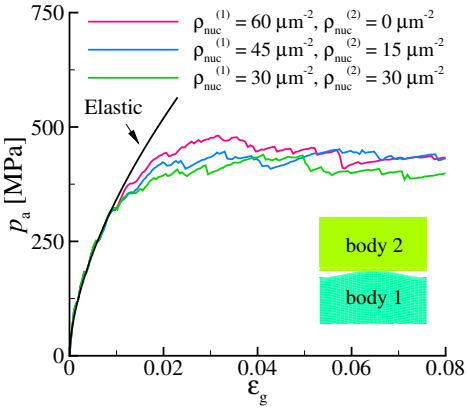

Figure 4.7: The mean apparent pressure for different density of sources in the bodies. The total source density is constant, $\rho_{\text{nuc}}^{(1)} + \rho_{\text{nuc}}^{(2)} = 60\,\mu\text{m}^{-2}$.

Figure 4.7 shows that the mean apparent pressure is unaffected by varying the source density in the bodies with the same $\rho_{\text{nuc}}^{(1)} + \rho_{\text{nuc}}^{(2)}$. The plastic response

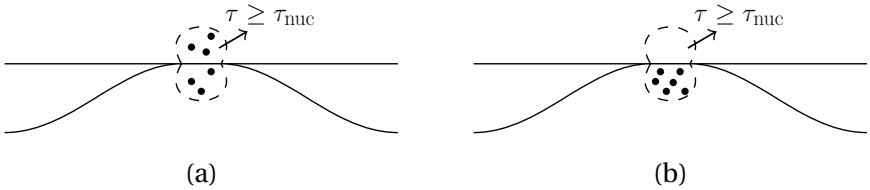

Figure 4.8: Schematics of sources (·) in the critical stress zone, $\tau > \bar{\tau}_{\text{nuc}}$, bounded by a dashed line for (a) both bodies with $\rho_{\text{nuc}}^{(1)} = \rho_{\text{nuc}}^{(2)}$ and (b) only the bottom body containing sources having a source density equal to $\rho_{\text{nuc}}^{(1)} + \rho_{\text{nuc}}^{(2)}$ of the bodies depicted in (a).

is similar because: (1) the critical elastic stress zone, where $\tau \geq \bar{\tau}_{\text{nuc}}$, has approximately the same size in both bodies, and (2) the dislocation sources are homogeneously distributed in one or both crystals. It follows that the density of dislocation sources in the critical stress zone depends on $\rho^{(1)}_{\text{nuc}} + \rho^{(2)}_{\text{nuc}}$ and not on the source density of each body (see Fig. 4.8). Those sources are the ones that sustain plastic deformation, and it is not relevant whether slip occurs only in one body or in both, only its total amount.

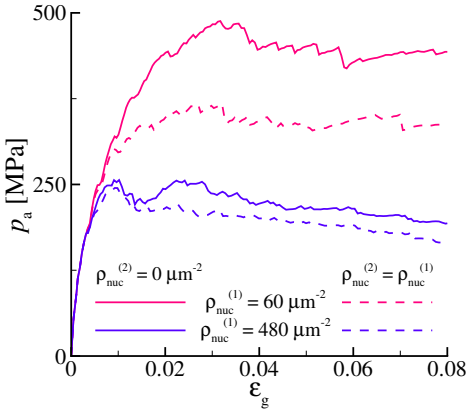

Figure 4.9: The apparent pressure with increasing $\rho^{(1)}_{\text{nuc}} + \rho^{(2)}_{\text{nuc}}$.

Clearly, increasing the total source density, $\rho^{(1)}_{\text{nuc}} + \rho^{(2)}_{\text{nuc}}$, will decrease the mean contact pressure, as can be seen in Fig. 4.9 where results are presented for $\rho^{(1)}_{\text{nuc}} + \rho^{(2)}_{\text{nuc}} = 60$, 120, 480 and $960 \mu\text{m}^{-2}$. Notice, however, that for the larger source density $\rho^{(1)}_{\text{nuc}} + \rho^{(2)}_{\text{nuc}} = 960 \mu\text{m}^{-2}$ the response is unaffected by increasing the number of sources (see the tiny difference between $\rho^{(1)}_{\text{nuc}} + \rho^{(2)}_{\text{nuc}} = 960 \mu\text{m}^{-2}$ and $\rho^{(1)}_{\text{nuc}} + \rho^{(2)}_{\text{nuc}} = 480 \mu\text{m}^{-2}$). This is because the number of sources is so large that the continuum limit is approached. At this limit, yield occurs in the material wherever the yield strength is exceeded due to the large availability of sources. This shows that the contact response is a function of the total source density only when the plastic behavior is source limited, but not in the continuum limit.

4.3.4. EFFECT OF OBSTACLES

The effect of changing the obstacle density ρ_{obs} on the mechanical response is next investigated. Only the obstacle density is varied, with $\rho_{\text{obs}} = 0 \mu\text{m}^{-2}$, $30 \mu\text{m}^{-2}$, $60 \mu\text{m}^{-2}$, $120 \mu\text{m}^{-2}$ and $240 \mu\text{m}^{-2}$. The obstacle strength is $\tau_{\text{obs}} = 150$ MPa. All other body properties are the same as in the previous section.

Figure 4.10a shows that only for $\rho_{\text{obs}} > 120 \mu\text{m}^{-2}$ the apparent contact pressure is larger. Although increasing ρ_{obs} decreases the average free path of dislo-

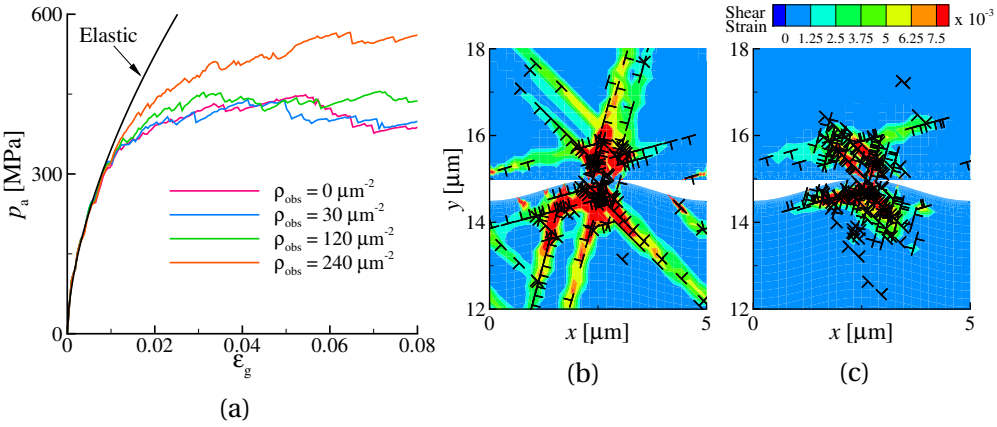

Figure 4.10: (a) Mean apparent pressure for bodies having different obstacle densities ρ_{obs}. Plastic shear strain and dislocation distributions for (b) $\rho_{\text{obs}} = 0\,\mu\text{m}^{-2}$ and (c) $\rho_{\text{obs}} = 240\,\mu\text{m}^{-2}$ at strain $\varepsilon_g = 7\,\%$.

cations (hence the slip provided by each dislocation), more dislocations are nucleated in response to the larger stresses, accounting for the required total glide. At larger obstacle densities however, the obstacle spacing d approaches the nucleation length L_{nuc} ($d < 3\,L_{\text{nuc}}$) of the dipole, greatly decreasing the distance a dislocation can glide right after it is nucleated, resulting in lesser slip and lesser stress relaxation. For instance at $\varepsilon_g = 7\,\%$, the magnitude and extent of plastic slip are much larger when $\rho_{\text{obs}} = 0\,\mu\text{m}^{-2}$ (Fig. 4.10b) than when $\rho_{\text{obs}} = 240\,\mu\text{m}^{-2}$ (Fig. 4.10c), even if the dislocation density is larger when $\rho_{\text{obs}} = 240\,\mu\text{m}^{-2}$.

A previous study of wedge indentation of a single crystal using discrete dislocation plasticity [34] also shows that the contact pressure is only marginally affected by the obstacle density. Therefore the obstacle density need not be considered when analyzing the mechanical response of contact between bodies that can deform by dislocation plasticity, provided the average obstacle spacing d is not too small compared with L_{nuc}: here $d > 3\,L_{\text{nuc}}$. The results are found also to apply for $\tau_{\text{obs}} \to \infty$.

4.3.5. EQUIVALENT SYSTEMS: MAPPING TWO PLASTIC BODIES IN CONTACT INTO A SINGLE PLASTIC BODY IN CONTACT WITH A RIGID BODY

CRYSTALS WITH THE SAME MATERIAL PROPERTIES

In this section, we explore the possibility of representing two plastically deformable bodies in contact by an equivalent system made of a rigid body in contact with a single plastically deformable body. The gap geometry and E' of the bodies in the equivalent system are the same as the two crystals in contact.

The contact pressure of two Al crystals is compared with the pressure obtained from the equivalent system. The deformable body in the equivalent system has $E = 35\,\text{GPa}$, to give $E' = 39.3\,\text{GPa}$, and a source density equal to the total source density, $\rho^{(1)}_{\text{nuc}} + \rho^{(2)}_{\text{nuc}}$, of the two crystals. This is because results from previous sections showed that the sources can be apportioned among the bodies without affecting the response, provided that the asperity is not too protruding (Sec. 4.3.2), and $\rho^{(1)}_{\text{nuc}} + \rho^{(2)}_{\text{nuc}}$ remains unchanged (Sec. 4.3.3). The obstacle density need not be considered (Sec. 4.3.4). All the other plastic properties are unchanged.

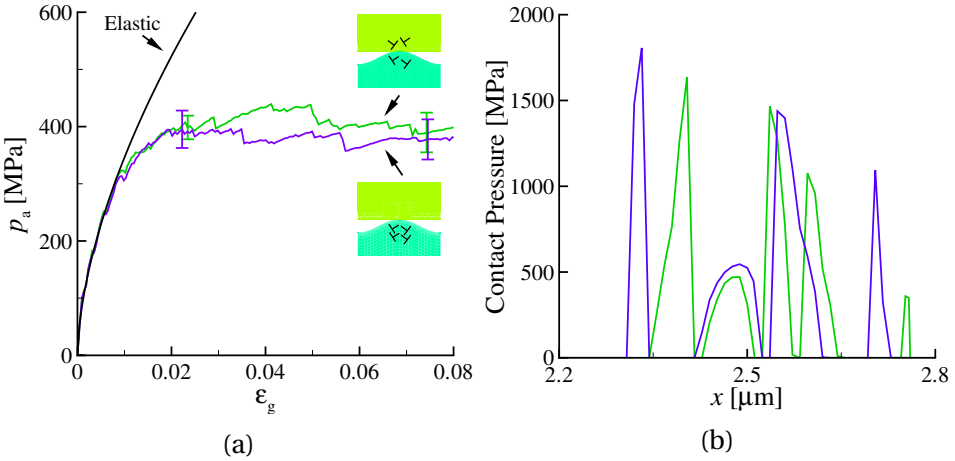

Figure 4.11: (a) Mean apparent pressure for two Al crystals in contact and contact between a rigid body and the single body with the same E' and gap geometry. (b) Contact pressure distribution at $\varepsilon_g = 7.5\,\%$ for a particular realization for both contact problems.

The mean apparent pressure in Fig. 4.11a shows a very good agreement between the response of the two bodies in contact and the equivalent system. The agreement is, as expected, less good in terms of contact pressure profiles, shown in Fig. 4.11b. Given the discrete nature of dislocations and slip planes the pressure peaks have a statistical character and cannot correspond one-to-one [11]. We observe a similar difference also when comparing pressure profiles for the same crystals in contact but different realizations.

Results show that two crystals of the same material in contact can be represented by an equivalent system of a rigid body in contact with a deformable body, provided that the gap geometry, E', and the total source density remain unchanged. This result also holds true in the continuum limit: the deformable body in the equivalent system will be described by the same constitutive plastic law as any of the bodies in the original problem.

CRYSTALS WITH DIFFERENT MATERIAL PROPERTIES IN CONTACT

The problem becomes more complicated when the materials in contact are different. Here, we simulate contact between a sinusoidal body having Al properties and a platen having Cu properties. The total source density of $\rho^{(1)}_{\text{nuc}} + \rho^{(2)}_{\text{nuc}} = 60\,\mu\text{m}^{-2}$.

Two equivalent systems are considered: (1) the deformable body has a source density $\rho_{\text{nuc}} = 60\,\mu\text{m}^{-2}$ and source strength of Al, $\bar{\tau}_{\text{nuc}} = 50\,\text{MPa}$, and (2) the deformable body has source density $\rho_{\text{nuc}} = 60\,\mu\text{m}^{-2}$ and source strength of Cu, $\bar{\tau}_{\text{nuc}} = 140\,\text{MPa}$.

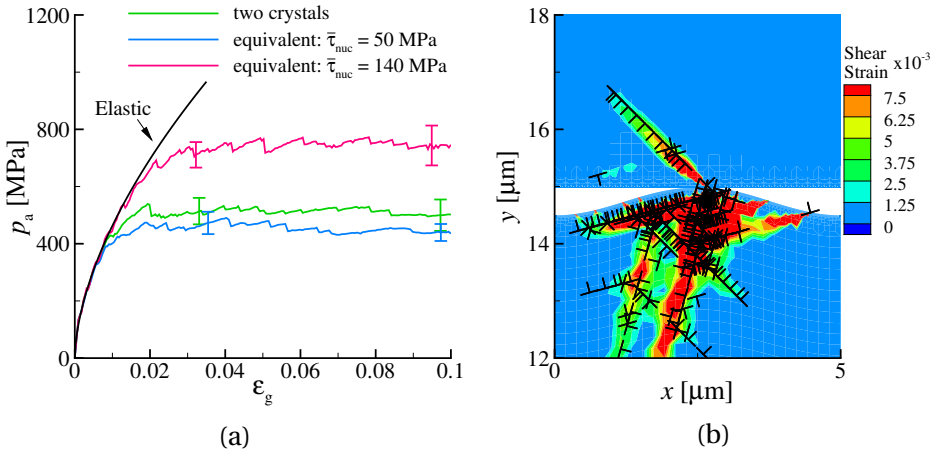

Figure 4.12: (a) The mean apparent pressure for two crystals in contact and the corresponding two equivalent systems identified by the average source strength $\bar{\tau}_{\text{nuc}}$ of the deformable body. (b) Plastic shear strain and dislocation distributions for contact between two crystals at $\varepsilon_g = 5\,\%$ for a particular realization.

The mean apparent pressure is given in Fig. 4.12a. The response obtained from the two equivalent systems differs greatly, and the difference involves only the onset of plasticity: at larger strains the slope of the pressure curves are approximately the same. The pressure difference is attributed to the much larger source strength τ_{nuc} of Cu as compared with Al, demonstrating also that the contact response is influenced mainly by the source strength τ_{nuc}, given the same total source density. The pressure of the two crystals in contact is however statistically the same as the single body having a source strength of Al in contact with a rigid body. This is because for the two crystals in contact, plastic slip occurs mainly in the Al crystal (see Fig. 4.12b).

Since for bodies with different material properties in contact the response is dominated by plastic activity in the body with a smaller source strength, we can simplify the two body problem into an equivalent problem of contact between

a deformable body and a rigid body, provided that the strength of the sources in the deformable body is that of the softer material. In continuum plasticity, this means that the deformable body in the simplified equivalent system should have the constitutive plastic law describing the softer material.

4.4. CONCLUSIONS

TWO dimensional discrete dislocation plasticity simulations of contact are performed for bodies that can both deform plastically. Here, we focus only on contact between a body with sinusoidal profile and a platen.

A size effect involving the onset of plasticity is present. This is attributed to source limitation in both bodies at the onset of plasticity, similar to what is observed in previous discrete dislocation plasticity simulations of contact where only the sinusoidal body deforms plastically. The contact response observed for two Al crystals in contact, and therefore also their size dependent response, is quantitatively similar to the contact response of two Cu crystals.

For (sub)-micrometer sized contacts, the contact response depends on the total sum of the source densities of both bodies, and not on how the dislocation sources are apportioned in the bodies. This holds provided that the sources are homogeneously distributed in each body, and that the asperities are not too steep.

Following the above result, and the observation that real surfaces have generally asperities that are not too protruding, we found that the problem of non-conformal contact between two metal crystals can be simplified into a problem of a single plastically deformable body in contact with a rigid body, provided that

- the gap geometry and the effective elastic modulus are the same,
- the source density of the single plastically deformable body is the same as the sum of the source densities of both bodies in the original problem,
- the strength of the sources in the single body is the source strength of the softer material of the two metal crystals in contact.

This simplification also holds in the continuum limit, where the deformable body in the equivalent problem should be modeled using the constitutive plastic law that describes the softer crystal.

It is therefore possible to use an equivalent system made of a single body in contact with a rigid platen to predict the plastic contact behavior of two metal crystals, which is advantageous since only one body is to be considered in the analysis, and the effects of the rigid body can be mimicked by a set of boundary conditions at the contact.

REFERENCES

[1] K. Ng Wei Siang and L. Nicola, *Contact between two plastically deformable crystals: a discrete dislocation dynamics study,* submitted to Philos. Mag. (2016).

[2] R. Maboudian, *Surface processes in MEMS technology,* Surf. Sci. Rrp. **30**, 207 (1998).

[3] L. De Chiffre, H. Kunzmann, G. N. Peggs, and D. A. Lucca, *Surfaces in precision engineering, microengineering and nanotechnology,* CIRP Ann. Manuf. Technol. **52**, 561 (2003).

[4] B. Bhushan, *Nanotribology and nanomechanics of MEMS/NEMS and bioMEMS/bioNEMS materials and devices,* Microelectron. Eng. **84**, 387 (2007).

[5] A. A. G. Bruzzone, H. L. Costa, P. M. Lonardo, and D. A. Lucca, *Advances in engineered surfaces for functional performance,* CIRP Ann. Manuf. Technol. **57**, 750 (2008).

[6] K. Komvopoulos, *Surface engineering and microtribology for microelectromechanical systems,* Wear **200**, 305 (1996).

[7] R. Maboudian, W. R. Ashurst, and C. Carraro, *Tribological challenges in micromechanical systems,* Tribol. Lett. **12**, 95 (2002).

[8] L. Nicola, A. F. Bower, K. S. Kim, A. Needleman, and E. Van der Giessen, *Multi-asperity contact: a comparison between discrete dislocation and crystal plasticity predictions,* Philos. Mag. **88**, 3713 (2008).

[9] F. Sun, E. Van der Giessen, and L. Nicola, *Plastic flattening of a sinusoidal metal surface: a discrete dislocation plasticity study,* Wear **296**, 672 (2012).

[10] F. Sun, E. Van der Giessen, and L. Nicola, *Interaction between neighboring asperities during flattening: a discrete dislocation plasticity analysis,* Mech. Mater. **90**, 157 (2015).

[11] K. Ng Wei Siang and L. Nicola, *Discrete dislocation plasticity analysis of contact between deformable bodies with simple geometry,* Model. Simul. Mater. Sci. **24**, 045008 (2016).

[12] C. Yang and B. N. J. Persson, *Molecular dynamics study of contact mechanics: contact area and interfacial separation from small to full contact,* Phys. Rev. Lett. **100**, 024303 (2008).

[13] Y. Mo and I. Szlufarska, *Roughness picture of friction in dry nanoscale contacts,* Phys. Rev. B **81**, 035405 (2010).

[14] S. Sandfeld and G. Po, *Microstructural comparison of the kinematics of discrete and continuum dislocations models,* Model. Simul. Mater. Sci. **23**, 085003 (2015).

[15] Y. S. Chen, W. Choi, S. Papanikolaou, M. Bierbaum, and J. P. Sethna, *Scaling theory of continuum dislocation dynamics in three dimensions: self-organized fractal pattern formation,* Int. J. Plas. **46**, 94 (2013).

[16] H. Gao and Y. Huang, *Geometrically necessary dislocation and size-dependent plasticity,* Scr. Mater. **48**, 113 (2003).

[17] A. Needleman and E. Van der Giessen, *Discrete dislocation and continuum descriptions of plastic flow,* Mater. Sci. Eng. A **309**, 1 (2001).

[18] J. R. Greer, W. C. Oliver, and W. D. Nix, *Size dependence of mechanical properties of gold at the micron scale in the absence of strain gradients,* Acta Mater. **53**, 1821 (2005).

[19] L. Nicola, Y. Xiang, J. J. Vlassak, E. Van der Giessen, and A. Needleman, *Plastic deformation of freestanding thin films: experiments and modeling,* J. Mech. Phys. Solids **54**, 2089 (2006).

[20] D. Kiener, W. Grosinger, G. Dehm, and R. Pippan, *A further step towards an understanding of size-dependent crystal plasticity: In situ tension experiments of miniaturized single-crystal copper samples,* Acta Mater. **56**, 580 (2008).

[21] K. N. Bachus, A. L. DeMarco, K. T. Judd, D. S. Horwitz, and D. S. Brodke, *Measuring contact area, force, and pressure for bioengineering applications: using Fuji Film and TekScan systems,* Med. Eng. Phys. **28**, 483 (2006).

[22] W. R. Chang, I. Etsion, and D. B. Bogy, *An elastic-plastic model for the contact of rough surfaces,* J. Tribol. T. ASME. **109**, 257 (1987).

[23] W. Yan and K. Komvopoulos, *Contact analysis of elastic-plastic fractal surfaces,* J. Appl. Phys. **84**, 3617 (1998).

[24] A. Majumdar and B. Bhushan, *Fractal model of elastic-plastic contact between rough surfaces,* J. Tribol. T. ASME. **113**, 1 (1991).

[25] L. Kogut and I. Etsion, *Elastic-plastic contact analysis of a sphere and a rigid flat,* J. Appl. Mech. **69**, 657 (2002).

[26] L. Kogut and I. Etsion, *A finite element based elastic-plastic model for the contact of rough surfaces,* Tribol. Trans. **46**, 383 (2003).

[27] L. Pei, S. Hyun, J. F. Molinari, and M. O. Robbins, *Finite element modeling of elasto-plastic contact between rough surfaces,* J. Mech. Phys. Solids **53**, 2385 (2005).

[28] B. N. J. Persson, *Elastoplastic contact between randomly rough surfaces,* Phys. Rev. Lett. **87**, 116101 (2001).

[29] B. N. J. Persson, *Contact mechanics for randomly rough surfaces,* Surf. Sci. Rrp. **61**, 201 (2006).

[30] L. Pastewka and M. O. Robbins, *Contact between rough surfaces and a criterion for macroscopic adhesion,* Proc. Natl. Acad. Sci. U.S.A. **111**, 3298 (2014).

[31] S. D. J. Mesarovic and N. A. Fleck, *Frictionless indentation of dissimilar elastic-plastic spheres,* Int J. Solids. Struct. **37**, 7071 (2000).

[32] R. L. Jackson and L. Kogut, *A comparison of flattening and indentation approaches for contact mechanics modeling of single asperity contacts,* J. Tribol. T. ASME. **128**, 209 (2006).

[33] Y. F. Gao, A. F. Bower, K. S. Kim, L. Lev, and Y. T. Cheng, *The behavior of an elastic-perfectly plastic sinusoidal surface under contact loading,* Wear **261**, 145 (2006).

[34] Y. Zhang, Y. F. Gao, and L. Nicola, *Lattice rotation caused by wedge indentation of a single crystal: dislocation dynamics compared to crystal plasticity simulations,* J. Mech. Phys. Solids **68**, 267 (2014).

5

STATIC FRICTION OF SINUSOIDAL ASPERITIES

Intelligence is the ability to adapt to change.

Stephen Hawking

Parts of this chapter are in an article submitted to Acta Mater. [1].

Discrete dislocation plasticity simulations are carried out to investigate the static frictional response of sinusoidal asperities with (sub)-microscale wavelength. The surfaces are first flattened and then sheared by a perfectly adhesive platen. Both bodies are explicitly modeled, and the external loading is applied on the top surface of the platen. Plastic deformation by dislocation glide is the only dissipation mechanism active. The tangential force obtained at the contact when displacing the platen horizontally first increases with applied displacement, then reaches a constant value. This constant is here taken to be the friction force.

In agreement with several experiments and continuum simulation studies, the friction coefficient is found to decrease with the applied normal load. However, at odds with continuum simulations, the friction force is also found to decrease with the normal load. The decrease is caused by an increased availability of dislocations to initiate and sustain plastic flow during shearing. Again in contrast to continuum studies, the friction coefficient is found to vary stochastically across the contact surface, and to reach locally values up to several times the average friction coefficient. Moreover, the friction force and the friction coefficient are found to be size dependent.

5.1. INTRODUCTION

FRICTION, as encountered in our everyday lives, is the resistance to relative motion between bodies in contact. Playing a major role in many applications, friction affects strongly the reliability and integrity of machines. This is especially true at the micron and smaller scale where the surface to volume ratio increases and surface effects become increasingly significant [2–4].

Several experiments show that the friction coefficient decreases with applied normal loading [5–8]. However, the results are controversial as other studies report a friction coefficient independent of applied loading [9–11]. It is not clearly understood whatcauses the different observed behavior since the results are very sensitive to the various experimental conditions. What is clear is that when interfacial cohesion is strong, friction is dependent on the material plastic properties, since the contact pressure is usually large enough for the asperities of the surface to deform plastically [12–14]. Several numerical models have been developed to analyze the effect of plastic deformation on friction of metallic surfaces [15–17]. These models consider a transition from elastic to full plastic deformation of the bodies in contact.

However, these local continuum static friction contact models lack a characteristic length scale and hence, they do not capture plasticity size effects [18], which are shown to be pronounced at the (sub)-micron scales [19–22]. Plasticity sets in at larger strains for smaller sized asperities. A larger tangential force is thus required to shear the micro-scale asperities then what would be predicted by a continuum model. This means that the friction force, and hence the friction coefficient could be underestimated by these local continuum friction models.

Although molecular dynamic simulations have been used to analyze contact behavior [23, 24] this technique becomes computationally too expensive when the dimensions of the bodies in contact are larger than a few nanometers. To address the contact problem at the micron scale studies using discrete dislocation plasticity (DDP) [25] have been carried out. This method bridges the gap between the atomic and the continuum scales since it accounts for the glide of individual dislocations, but neglects atomic vibrations. By that the model contains the intrinsic length scale of plasticity: the Burgers vector.

So far discrete DDP studies of friction were confined to a single asperity on top of a large body. However, the behavior of micro-scale multi-asperity contacts studied by DDP was found to be different from that of a single asperity contact: the mean contact pressure during flattening decreases with decreasing asperity size and spacing [26–29]. Also, when three adjacent asperities are collectively sheared the mean contact shear stress is smaller than when only a single isolated asperity is sheared [30]. Here, we analyze for the first time, using DDP, the static

frictional response of a sinusoidal surface. Loading is applied on the top surface of the contacting platen. The bodies are pre-loaded with a constant normal force applied on the platen before shearing. The friction coefficient can so be directly determined. Notice that this is not possible when a constant normal displacement is applied since the normal force will decrease during shearing [31], making it hard to define a unique friction coefficient.

We here examine how the friction force and the friction coefficient vary with the normal force applied, when plastic flow by discrete dislocations is the unique dissipation process. The dependence of the friction force and the friction coefficient on the wavelength of the sinusoidal is also explored.

5.2. PROBLEM DESCRIPTION

The contact problem is schematically represented in Fig. 5.1. The bottom crystal has a sinusoidal surface profile, with a wavelength λ and an amplitude φ_0. Each sinusoid represents a surface asperity. The top crystal has a flat surface profile.

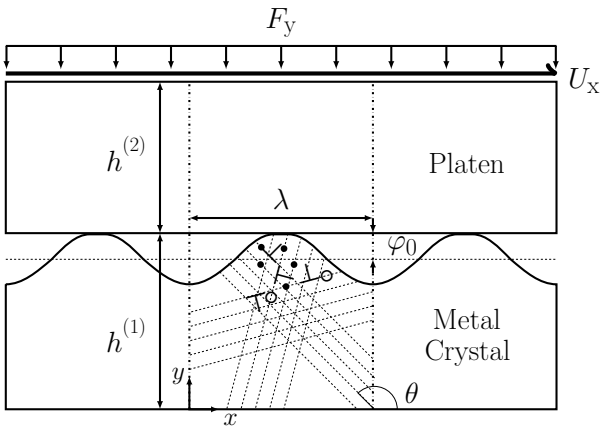

Figure 5.1: Two-dimensional model of a metal single crystal with sinusoidal surface sheared by a platen that is subjected to a uniform distributed normal load F_y. Dislocations $(\top, \perp)$ are nucleated from sources $(\cdot)$ homogeneously distributed in the bottom crystal, which contains also randomly distributed obstacles $(\circ)$.

The bottom and top crystals have heights $h^{(1)} - \varphi_0$ and $h^{(2)}$ respectively, where $\varphi_0 \lll h^{(1)}$. Given the periodicity of the surface, a representative unit cell with wavelength λ is here considered. The bottom crystal undergoes plastic deformation by edge dislocations gliding along slip planes oriented at an angle θ_i to the x direction. Based on the two dimensional representation of the FCC crystal structure [32], three sets of slip planes are considered, oriented at $\theta_1 = 15°, \theta_2 = 75°$ and $\theta_3 = 135°$. These orientations are chosen to avoid alignment of the slip

planes with the loading directions, which might lead to unrealistic softening of the crystal. The slip planes with the same orientation θ are spaced $200b$ apart.

Dislocation sources and obstacles are homogeneously distributed throughout the initially dislocation and stress free body, and they have a density of $\rho_{\text{nuc}} = 60\,\mu\text{m}^{-2}$ and $\rho_{\text{obs}} = 30\,\mu\text{m}^{-2}$, respectively, unless otherwise stated. The sources have a strength τ_{nuc} normally distributed with a mean of 50 MPa and a standard deviation of 20 %, and a nucleation time t_{nuc} of 10 ns. The obstacle strength τ_{obs} is 150 MPa. The dislocations have a Burgers vector of $b = 2.5\,\text{Å}$, and they glide in the material with a velocity v directly related to the resolved Peach Koehler force f_{p} through the drag coefficient $D = 10^{-10}\,\text{MPa s}$.

5.2.1. BOUNDARY CONDITIONS

An external normal force is first applied incrementally on the top surface of the platen up to

$$F_{\text{y}} = \int_0^{t_{\text{f}}} \dot{F}_{\text{y}}\,\mathrm{d}t = T_{\text{y}}(t_{\text{f}})\lambda, \tag{5.1}$$

where $\dot{F}_{\text{y}}$ and T_{y} are the normal force rate and the uniformly distributed normal traction, respectively. Next, a uniform horizontal displacement U_{x} is applied:

$$U_{\text{x}} = \int_{t_{\text{f}}}^{t} \dot{U}_{\text{x}}\,\mathrm{d}t, \tag{5.2}$$

Periodic boundary conditions are imposed on the lateral sides of the unit cell, $\mathbf{u}(0,y) - \mathbf{u}(\lambda,y) = 0$. At the base of the bottom crystal $\mathbf{u}(x,0) = 0$. For these two dimensional plane strain simulations the quantities given are per unit depth of the crystals, and here the unit of depth in our variables is omitted.

5.3. PRELIMINARY RESULTS: CHOICE OF THE SIMULATION CELL DIMENSIONS

THESE simulations aim at capturing plastic deformation in the subsurface region of a large metal crystal. First, we make sure that the periodic unit cell is chosen with a sufficiently large width-to-height aspect ratio to not undergo unrealistic plastic shearing from the top to the bottom. To this end, simulations are here performed for a unit cell containing an asperity with wavelength $\lambda = 2.5\,\mu\text{m}$. The responses for two different heights of the cell, $h = 15\,\mu\text{m}$ and $30\,\mu\text{m}$ are then compared. The asperity amplitude is $\varphi_0 = 0.1\,\mu\text{m}$. Here, we consider the deformable body to have elastic isotropic properties of Al, $E = 70\,\text{MPa}$ and $\nu = 0.33$. The platen is rigid, and has a Young modulus $E = 10^6\,E^{(\text{Al})}$; the platen modulus

is sufficiently small to prevent ill-conditioning of the finite element stiffness matrix. The mean shear response is independent of the number of (periodic) unit cells simulated (not shown here). A normal force is applied incrementally on the top surface of the platen up to a value of $F_y/\lambda = 30\,\mathrm{N}/\mu\mathrm{m}$ before applying a tangential displacement.

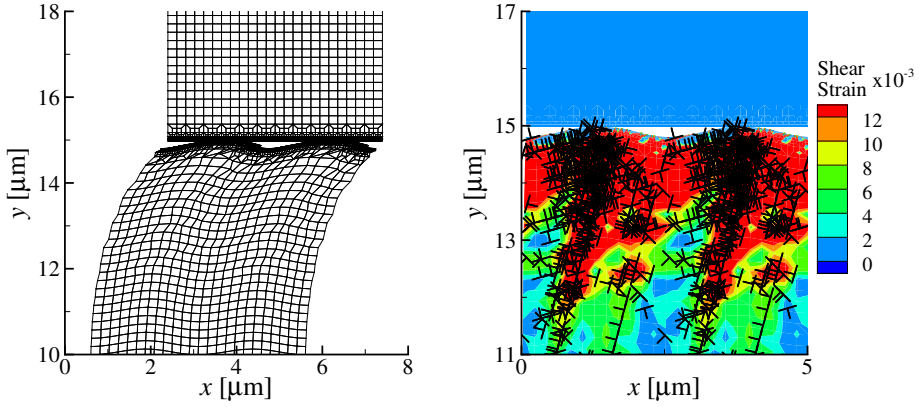

Figure 5.2: (a) Deformed mesh plot for a body with height $h = 15\,\mu$m at $U_x = 0.07\,\mu$m. Two identical unit cells are presented to show clearly the region where plasticity occurs. Displacements in the x direction are magnified 30 times. (b) Corresponding plastic strain distribution at the same U_x.

Inspection of the deformed mesh (x displacements magnified 30 times) for height $h = 15\,\mu$m in Fig. 5.2a shows that only a region of about $4\,\mu$m underneath the contact is greatly deformed. To examine where slip occurs in the material, the corresponding plastic shear strain distribution of the bodies is presented in Fig. 5.2b. The plastic shear strain at each material point is calculated as the sum of the shear strains along each slip direction. Only the region $4\,\mu$m underneath the contact of the bottom body is shown, where more than 90% of the dislocations are found. Indeed, a large amount of slip occurs near the contact, indicating that the tangential force applied only shears the asperities and a small region (a couple of μm in depth) beneath the surface.

The tangential force $F_x = \int_{\Gamma\in\gamma_c} \mathbf{T}\cdot\mathbf{n}_x\,\mathrm{d}\Gamma$ is next shown in Fig. 5.3 as a function of tangential displacement U_x for two different crystal heights, $h = 15\,\mu$m and $h = 30\,\mu$m. The curves for both heights deviate from the elastic curves at small U_x because dislocations are already nucleated during flattening, and they are available to glide and assist in plastic shearing [30]. Initially the tangential force F_x at each U_x is smaller for bodies with larger height but at larger displacements ($U_x > 0.04\,\mu$m) the tangential force F_x levels off at approximately the same value for both heights considered.

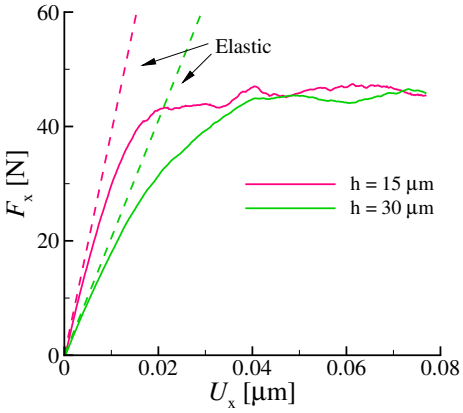

Figure 5.3: Tangential force F_x against displacement U_x for bodies with two different heights.

Evidently, the plastic shear response at larger displacement is unaffected by the height of the unit cell. Therefore, in subsequent sections only deformable bodies with $h = 15\,\mu$m will be considered, to lower the computational cost.

5.4. SHEARING WITH AN ELASTIC OR A PLASTIC PLATEN

NEXT we investigate how the tangential force F_x depends on whether the platen is rigid, or can deform elastically, or plastically. Sinusoidal asperities with a wavelength $\lambda = 5.0\,\mu$m and an amplitude $\varphi_0 = 0.2\,\mu$m are considered. When the platen is elastically deformable it has Poisson ratio $\nu = 0.33$ and elastic modulus either $E = 70$ GPa, or $E = 35$ GPa. When it can deform plastically, both the platen and the body with sinusoidal surface have the same source density, $\rho_{\text{nuc}} = 30\,\mu\text{m}^{-2}$, and an elastic modulus of $E = 70$ GPa.

Figure 5.4 shows the tangential force F_x as a function of plastic displacement U_{xp} after flattening the bodies to a normal force $F_y = 150$ N. In the initial stages of shearing, i.e. $U_{xp} \leq 0.025\,\mu$m, the curves do not overlap because plasticity already occurs during flattening. At larger U_{xp}, the tangential force F_x is found to be approximately the same when the platen is rigid, elastic, or plastic. Evidently, the shear response does not depend on whether plasticity is confined to one body or occurs in both. The plastic shear and dislocation distributions for the elastic platen and plastic platen are shown in Fig. 5.5a and Fig. 5.5b.

As to be expected, increasing the source density of the bodies to $\rho^{(1)}_{\text{nuc}} = \rho^{(2)}_{\text{nuc}} = 60\,\mu\text{m}^{-2}$ decreases the tangential force F_x . Further increasing the source density should lead to the continuum limit, which is represented in Fig. 5.4 by the response obtained using the crystal plasticity model proposed by Peirce *et al.* [33].

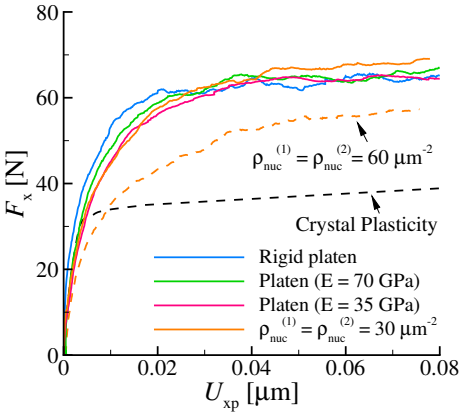

Figure 5.4: Horizontal force F_x against plastic displacement U_{xp} for bodies with different properties. The force obtained from crystal plasticity is also included.

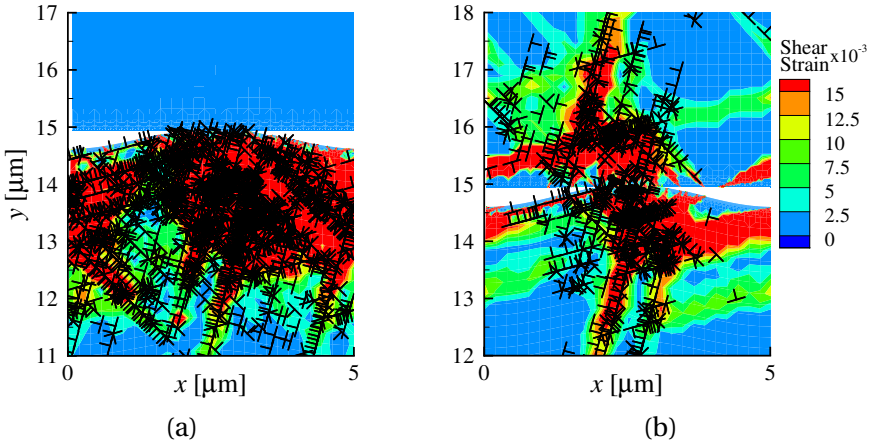

Figure 5.5: Plastic strain distribution for shearing using an elastic platen with (a) $E = 70\,\text{GPa}$ and (b) shearing both bodies, each having a source density of $30\,\mu\text{m}^{-2}$, at plastic displacement $U_{xp} = 0.06\,\mu\text{m}$ for a particular realization.

5.5. EFFECT OF NORMAL LOADING ON THE SHEAR RESPONSE

IN the following section we will investigate how the friction force is affected by pre-loading the bodies with different normal force F_y. The friction force F_f is defined as the constant tangential force resisting relative sliding between the surfaces in contact. In this work however, there is no sliding at the contact, but only plastic flow in the material underneath the contact. Given that here after a certain U_x the tangential force approaches a constant value, the tangential force at displacement $U_x = 0.08\,\mu\text{m}$ is taken as the friction force.

During normal loading, the contact area and the elastic stresses induced by the normal force, as well as the plasticity generated during flattening affect the tangential force required to shear the asperities. The effect of each of these factors on the friction force is separately analyzed in the following subsections.

5.5.1. CONTACT AREA

The effect of the contact area A on F_x is first investigated. To have a contact area without applying a normal force before shearing, the sinusoidal asperity with $\lambda = 5.0\,\mu$m and $\varphi_0 = 0.2\,\mu$m is truncated at a depth from the apex. Three contact areas $A = 0.1\,\mu$m, $0.5\,\mu$m and $1.0\,\mu$m are considered. Given that the plastic shear response is independent of the compliance of the platen, we take the platen to be rigid.

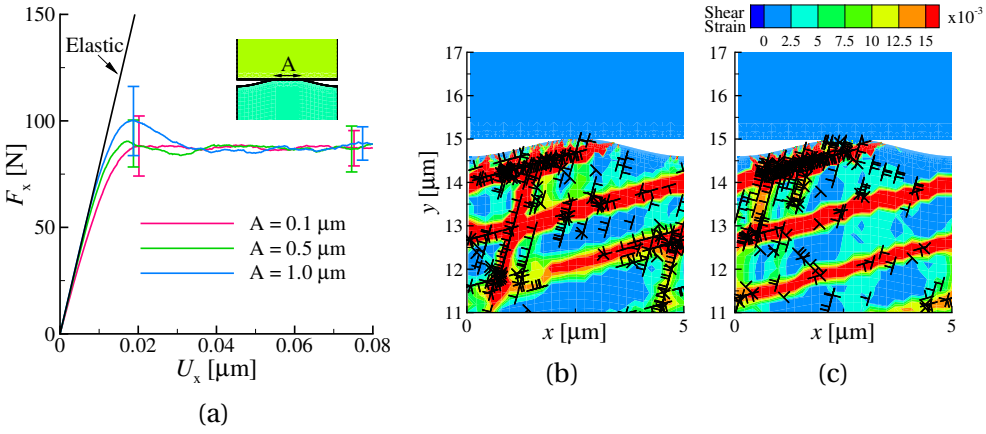

Figure 5.6: (a) Tangential force F_x of a truncated sinusoidal surface for different contact areas A. Each vertical bar corresponds to the standard deviation of eight simulations. Plastic shear strain and dislocation distributions for a particular realization for A = (b) $0.1\,\mu$m and (c) $1.0\,\mu$m at $U_x = 0.08\,\mu$m.

Figure 5.6a shows the tangential force F_x as a function of the tangential displacement U_x. The elastic shear responses for the different areas are approximately the same. Apparently, the friction force F_f is unaffected by the size of the contact area. This is because the contact areas considered are small and much smaller than the plastic region underneath the contact. Inspection of the plastic shear strain distribution in the crystals for both $A = 0.1\,\mu$m (Fig. 5.6b) and $1.0\,\mu$m (Fig. 5.6c) at $U_x = 0.08\,\mu$m shows indeed on average, similar distinct shear bands whose dimensions are much larger than (and non related to) the contact area.

5.5.2. EFFECT OF ELASTIC FLATTENING

To investigate the effect of elastic normal loading on the friction force three normal forces $F_y = 50\,\text{N}, 100\,\text{N}$ and $120\,\text{N}$ are first applied on the truncated asperity surface with $A = 1.0\,\mu\text{m}$ before the surface is tangentially displaced. The chosen area is sufficiently large that no plasticity occurs during flattening. Figure 5.7

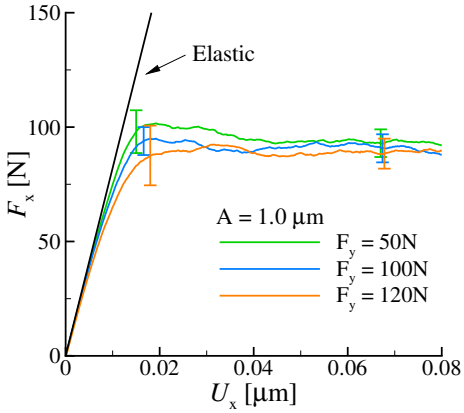

Figure 5.7: Tangential force F_x for different normal loads F_y applied on an area of $A = 1.0\,\mu\text{m}$. Each vertical bar corresponds to the standard deviation of eight simulations.

shows that the tangential force is approximately the same for the different values of the applied normal force. Clearly, the elastic normal loading does not affect the plastic shear response of the asperities.

5.5.3. EFFECT OF PLASTIC FLATTENING

We examine next the effect of plasticity induced during flattening on the tangential force by first loading the sinusoidal asperities with $\lambda = 5.0\,\mu\text{m}$ and $\varphi_0 = 0.2\,\mu\text{m}$ with a constant normal force before applying a tangential displacement. Six values for the normal force, $F_y = 25\,\text{N}, 50\,\text{N}, 100\,\text{N}, 150\,\text{N}, 200\,\text{N}$ and $250\,\text{N}$, are considered, indicated by dots in Fig. 5.8a, which gives the normal displacement U_y against the normal force. The increase of the tangential force F_x during shearing is presented in Fig. 5.8b for the various normal loads. For normal loads $F_y \leq 50\,\text{N}$, the curves overlap, since flattening is still elastic (see Fig. 5.8a). When the asperities are pre-loaded with a larger normal force, dislocations are nucleated during flattening, and F_x deviates from the elastic response at a smaller U_x: the tangential force also levels off at a smaller value. However, the tangential force does not further decrease when the normal force is increased from $200\,N$ to $250\,N$.

For normal force $F_y > 50\,\text{N}$ dislocations generated during flattening assist in

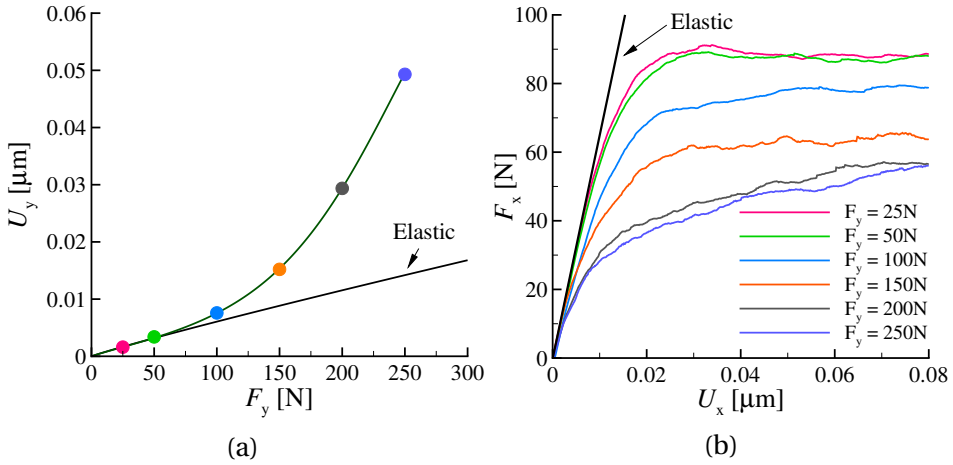

Figure 5.8: (a) Normal displacement U_y with normal force F_y. The dots represent the normal force the asperities are pre-loaded with, before they are sheared. (b) Tangential force F_x as a function of U_x.

5

plastic shearing. The tangential force required to shear the asperities is therefore decreased with increasing normal force. However, when the normal force is further increased beyond $F_y = 200\,N$, plastic flow in the region underneath the contact caused by flattening approaches an upper limit, and therefore does not further facilitate plastic shearing of the sinusoidal asperities. This leads to approximately the same plastic slip during shear (not shown here) for $F_y = 200\,N$ and $250\,N$.

5.5.4. FRICTION FORCE AND THE FRICTION COEFFICIENT

Results of the previous section are compiled in Fig. 5.9 to show the variation of the friction force F_f and the friction coefficient $\mu = F_f/F_y$ with the normal force. Both the friction force and the friction coefficient decrease when the normal force is increased. When the applied normal force is small, for $F_y \leq 100\,N$, the friction coefficient μ obtained from our simulations is larger than typical experimental values, which range from 0.3 to 1.4 for various materials and conditions (see e.g. [34]). At larger applied normal force however, the friction force becomes smaller as plastic shearing is assisted by dislocations generated during flattening. This decreases the friction coefficient to within the experimental range.

The decrease of the friction coefficient with increasing normal load is also observed in local continuum plasticity studies of static friction (e.g. [15–17]). However, the friction force there increases sub-linearly with the normal force, which contrasts our results. The reason for this discrepancy is that in the continuum

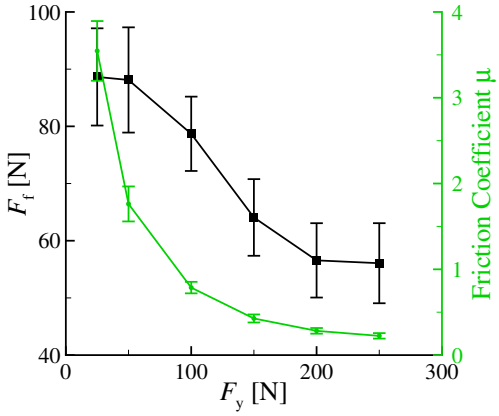

Figure 5.9: Friction force F_f and the corresponding friction coefficient $\mu = F_f/F_y$ for the results shown in Fig. 5.8b.

study the contact area increases significantly with increasing normal load, determining an increase of the friction force. In the DDP simulations the contact area increases only negligibly.

LOCAL FRICTION COEFFICIENT

Although a uniform distributed normal traction t_y is applied on the top surface of the platen the tangential traction t_x^c and the normal traction t_y^c at the contact are highly non-uniform, as seen in Fig. 5.10a, which shows the tractions t_x^c and t_y^c along the contact for $F_y = 200\,\text{N}$ at displacement $U_x = 0.08\,\mu\text{m}$. This is because the contact is patchy (Fig. 5.10b), a consequence of the discrete nature of dislocations and slip planes [28]. The local tractions can be either positive or negative, since the contact is full stick and dislocations have opposite orientation on different slip planes.

Although t_x^c is, on average, smaller than t_y^c, and the average friction coefficient μ is about 0.23, the local friction coefficient $|t_x^c/t_y^c|$ can be as large as 1.0 (Fig. 5.10c). Other realizations show similar characteristics. The average friction coefficient μ is not correlated to the local friction coefficient across the contact.

The discontinuous variation of the local friction coefficient across the contact is not observed in local continuum static friction studies (see e.g. [16]), where the contact area is continuous.

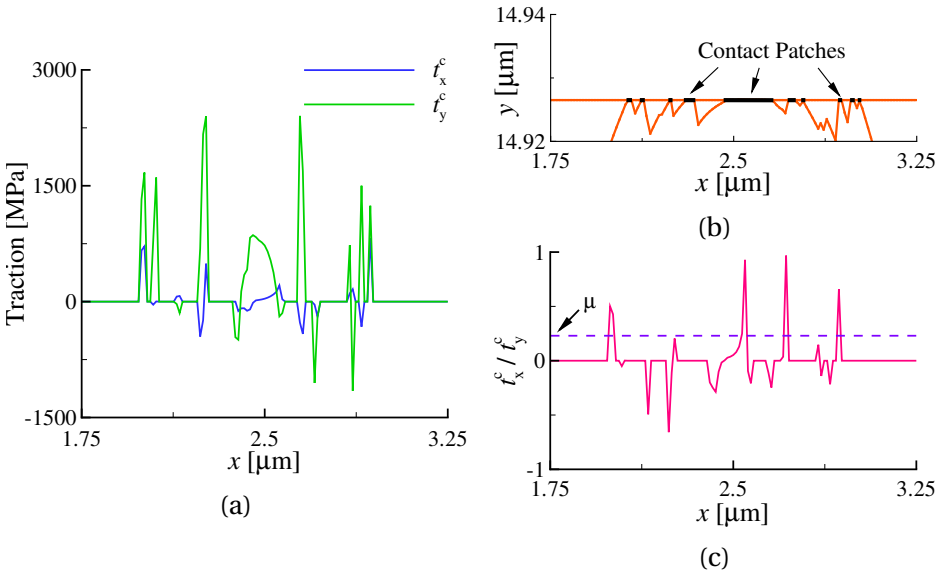

Figure 5.10: (a) Contact traction distribution t^c in the x and y directions for $F_y = 200\,N$ at $U_x = 0.08\,\mu m$ for a particular realization. (b) Corresponding contact profile: the y axis is stretched independently of the x axis, and (c) the ratio t_x^c / t_y^c. The average value of the friction coefficient is shown using a dashed line.

5.6. FRICTION FORCE OF SCALED ASPERITIES

IN this section, we investigate how the friction force is affected by the size of the sinusoidal asperities. Two scaled asperities having $\lambda = 2.5\,\mu m$ and $5.0\,\mu m$, both with an aspect ratio $\lambda/\varphi_0 = 25$ are considered. The bodies are pre-loaded with different values of the normal force. The elastic response of the scaled asperities is identical, so that a direct comparison can be made when presenting tangential force against normal force if they are both divided by the wavelength λ as in Fig. 5.11a. The mean friction force per unit wavelength of the smaller asperities is larger, especially at large F_y/λ. Also, the decrease of friction force with normal force for the smaller asperities is less than for the larger. The corresponding friction coefficient μ in Fig. 5.11b, is therefore larger for the smaller asperities. For instance, μ for asperities with $\lambda = 2.5\,\mu m$ at $F_y/\lambda = 40\,N/\mu m$ is approximately 1.6 times larger than that of asperities with $\lambda = 5.0\,\mu m$.

The size effect of the friction force and the friction coefficient observed in the simulations here is a result of a plasticity size effect in flattening. Deformation becomes increasingly source limited when the asperity size decreases [26, 28, 29]. Plastic shear is less assisted given the smaller amount of plasticity generated in the smaller asperity during flattening, resulting in a smaller decrease in F_f/λ when F_y/λ is increased than for the larger asperity.

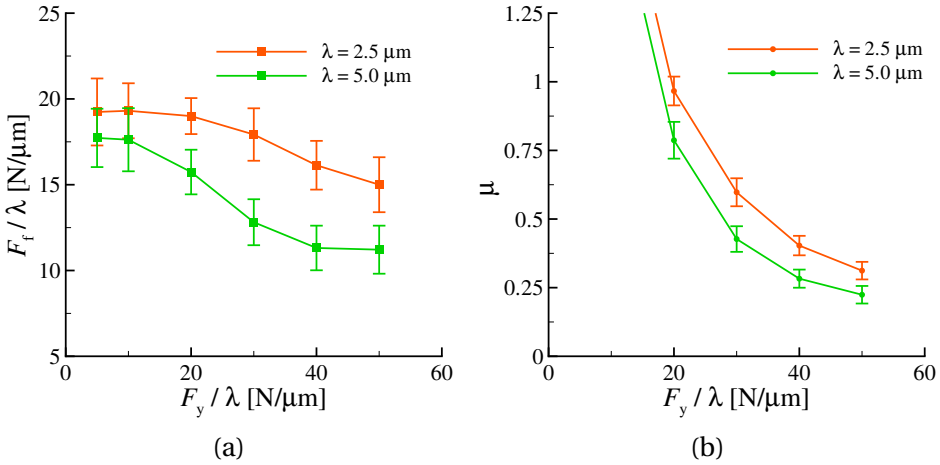

Figure 5.11: (a) Friction force per unit wavelength F_f/λ, and (b) corresponding friction coefficient as a function of normal force per unit wavelength F_y/λ for asperity wavelengths $\lambda = 2.5\,\mu$m and $5.0\,\mu$m. Each vertical bar corresponds to the standard deviation of eight simulations.

5.7. CONCLUSIONS

TWO dimensional discrete dislocation plasticity simulations are performed to investigate the static friction response of sinusoidal surfaces in full stick contact with a platen. A normal force is first applied on the top surface of the platen before shearing starts. After an initial increase the tangential force at the contact reaches a constant value, which is here taken to be the static friction force.

Results show that the value of the friction force does not depend on whether the platen is rigid, elastic, or even plastic, as long as the plastic properties of the platen are the same as those of the sinusoidal body.

The friction force is also independent of the size of the contact area, which is anyhow rather small in these simulations, below $1\,\mu$m. An applied normal load has an effect on the friction force only when it is sufficiently large to induce plasticity. If this is the case the friction force decreases with the applied normal force. This is because dislocations, generated during flattening, assist in plastic shearing, which results in the decrease of the friction force when the applied normal force is increased. When plastic flow caused by flattening reaches an upper limit, increasing the normal load further no longer affects the friction force.

Given the decrease in the friction force, the friction coefficient decreases with increasing normal load. The decrease in the friction coefficient is similarly observed in experiments and local continuum plasticity studies of static friction. However, the decrease of friction coefficient in the continuum plasticity studies is caused by a sub-linear increase of the friction force with load. The increase is

due to a significant increase in contact area.

The discrete dislocation plasticity simulations presented here display two other differences with the local continuum plasticity studies: (1) a discontinuous variation of the local friction coefficient along the contact, which can be up to five times larger than the average friction coefficient, and (2) the size dependence of the friction force and coefficient displayed by sinusoids with different wavelength.

REFERENCES

[1] K. Ng Wei Siang and L. Nicola, *Static friction of sinusoidal surfaces: a discrete dislocation plasticity analysis,* submitted to Acta Mater. (2016).

[2] B. Bhushan, *Fundamentals of tribology and bridging the gap between the macro-and micro/nanoscales*, Vol. 10 (Springer Science & Business Media, 2001).

[3] M. Urbakh, J. Klafter, D. Gourdon, and J. Israelachvili, *The nonlinear nature of friction,* Nat. **430**, 525 (2004).

[4] N. S. Tambe and B. Bhushan, *Scale dependence of micro/nano-friction and adhesion of MEMS/NEMS materials, coatings and lubricants,* Nanotechnol. **15**, 1561 (2004).

[5] E. Rabinowicz, *Friction coefficients of noble metals over a range of loads,* Wear **159**, 89 (1992).

[6] I. Etsion and M. Amit, *The effect of small normal loads on the static friction coefficient for very smooth surfaces,* J. Tribol. T. ASME. **115**, 406 (1993).

[7] U. D. Schwarz, W. Allers, G. Gensterblum, and R. Wiesendanger, *Low-load friction behavior of epitaxial c 60 monolayers under hertzian contact,* Phys. Rev. B **52**, 14976 (1995).

[8] A. Ovcharenko, G. Halperin, and I. Etsion, *Experimental study of adhesive static friction in a spherical elastic-plastic contact,* J. Tribol. T. ASME. **130**, 021401 (2008).

[9] Q. Chen and G. P. Carman, *Microscale tribology (friction) measurement and influence of crystal orientation and fabrication process,* in *Proc. 13th Annu. Int. Conf. Micro Electro Mech. Syst.* (IEEE, 2000) pp. 657–661.

[10] D. Gourdon and J. N. Israelachvili, *Transitions between smooth and complex stick-slip sliding of surfaces,* Phys. Rev. E **68**, 021602 (2003).

[11] L. Bureau, C. Caroli, and T. Baumberger, *Frictional dissipation and interfacial glass transition of polymeric solids,* Phys. Rev. Lett. **97**, 225501 (2006).

[12] F. P. Bowden and D. Tabor, *The nature of sliding and the analysis of friction,* Proc. R. Soc. London, Ser. A **169**, 371 (1939).

[13] S. Hyun, L. Pei, J. F. Molinari, and M. O. Robbins, *Finite-element analysis of contact between elastic self-affine surfaces,* Phys. Rev. E **70**, 026117 (2004).

[14] R. Jedynak and M. Sułek, *Numerical and experimental investigation of plastic interaction between rough surfaces,* Arab J. Sci. Eng. **39**, 4165 (2014).

[15] L. Kogut and I. Etsion, *A static friction model for elastic-plastic contacting rough surfaces,* J. Tribol. T. ASME. **126**, 34 (2004).

[16] V. Brizmer, Y. Kligerman, and I. Etsion, *Elastic–plastic spherical contact under combined normal and tangential loading in full stick,* Tribol. Lett. **25**, 61 (2007).

[17] I. Etsion, *Revisiting the* C*attaneo*-M*indlin concept of interfacial slip in tangentially loaded compliant bodies,* J. Tribol. T. ASME. **132**, 020801 (2010).

[18] B. Luan and M. O. Robbins, *The breakdown of continuum models for mechanical contacts,* Nat. **435**, 929 (2005).

[19] J. R. Greer and W. D. Nix, *Size dependence of mechanical properties of gold at the sub-micron scale,* Appl. Phys. A **80**, 1625 (2005).

[20] L. Nicola, Y. Xiang, J. J. Vlassak, E. Van der Giessen, and A. Needleman, *Plastic deformation of freestanding thin films: experiments and modeling,* J. Mech. Phys. Solids **54**, 2089 (2006).

[21] D. Kiener, W. Grosinger, G. Dehm, and R. Pippan, *A further step towards an understanding of size-dependent crystal plasticity: in situ tension experiments of miniaturized single-crystal copper samples,* Acta Mater. **56**, 580 (2008).

[22] J. R. Greer and J. T. M. De Hosson, *Plasticity in small-sized metallic systems: intrinsic versus extrinsic size effect,* Prog. Mater. Sci. **56**, 654 (2011).

[23] L. C. Zhang, K. L. Johnson, and W. C. D. Cheong, *A molecular dynamics study of scale effects on the friction of single-asperity contacts,* TL **10**, 23 (2001).

[24] Y. Dong, Q. Li, and A. Martini, *Molecular dynamics simulation of atomic friction: a review and guide,* J. Vac. Sci. Technol. A **31**, 030801 (2013).

[25] E. Van der Giessen and A. Needleman, *Discrete dislocation plasticity: a simple planar model,* Model. Simul. Mater. Sci. **3**, 689 (1995).

[26] F. Sun, E. Van der Giessen, and L. Nicola, *Plastic flattening of a sinusoidal metal surface: a discrete dislocation plasticity study,* Wear **296**, 672 (2012).

[27] L. Nicola, A. F. Bower, K.-S. Kim, A. Needleman, and E. Van der Giessen, *Multi-asperity contact: A comparison between discrete dislocation and crystal plasticity predictions,* Philos. Mag. **88**, 3713 (2008).

[28] K. Ng Wei Siang and L. Nicola, *Discrete dislocation plasticity analysis of contact between deformable bodies with simple geometry,* Model. Simul. Mater. Sci. **24**, 045008 (2016).

[29] K. Ng Wei Siang and L. Nicola, *Contact between two plastically deformable crystals: a discrete dislocation dynamics study,* submitted to Philos. Mag. (2016).

[30] F. Sun, E. Van der Giessen, and L. Nicola, *Effect of plastic flattening on the shearing response of metal asperities: a dislocation dynamics analysis,* J. Appl. Mech. **82**, 071009 (2015).

[31] H. Song, R. J. Dikken, L. Nicola, and E. Van der Giessen, *Plastic ploughing of a sinusoidal asperity on a rough surface,* J. Appl. Mech. **82**, 071006 (2015).

[32] J. R. Rice, *Tensile crack tip fields in elastic-ideally plastic crystals,* Mech. Mater. **6**, 317 (1987).

[33] D. Peirce, R. J. Asaro, and A. Needleman, *Material rate dependence and localized deformation in crystalline solids,* Acta Metall. **31**, 1951 (1983).

[34] F. Cardarelli, *Materials handbook: a concise desktop reference* (Springer Science & Business Media, 2008).

6

Concluding Remarks

Without a belief that it is possible to embrace
the reality with our theoretical models,
there could be no science.
This belief is, and always will be,
the main motive of all scientific work.

Albert Einstein

6.1. CONCLUSIONS

FROM this thesis we gained a better understanding of the mechanical behavior of two bodies with rough surfaces in contact that can both deform by dislocation plasticity. A contact model is developed to simulate two plastically deformable bodies in contact. Plasticity is described as the collective glide of edge dislocations. Although the model is general, we first confine our analysis to two dimensional simulations of the contact between a plastically deformable body with sinusoidal surface and a rigid platen (Chapter 3), to investigate the effect of contact conditions, i.e. full stick or frictionless. We find that the true area of contact, hence the local contact pressure distribution, are strongly dependent on the contact conditions. Contact is more patchy for frictionless contacts compared with full stick contacts, resulting also in larger pressure peaks for frictionless contact. This is because dislocations can glide through the contact regions only in the case of frictionless contacts.

Previous discrete dislocation plasticity studies of contact do not capture this effect because dislocations do not escape the contact, even when the contact is frictionless. This is so to preserve compatibility of the applied boundary conditions at the contact.

However, despite the large differences in the true contact area observed for frictionless and sticking contacts, the apparent contact area, apparent contact pressure and plastic deformation in the crystal are unaffected by the contact conditions. The exact morphology of the true contact area does not affect the plastic slip in the body. This is attributed to the fact that the spacing between patches is very small, smaller than the average dislocation source spacing.

We also demonstrate, in the same chapter, a size effect when the sinusoidal body is flattened either by a rigid or an elastic platen, i.e. smaller asperities support a larger pressure than larger asperities. The size dependence involves only the onset of plasticity and is attributed to source limitation: at larger strains, the effect of source limitation disappears as more dislocations are generated, and the mean contact pressure is approximately constant with increasing strain. The size effect however, becomes less pronounced when the compliance of the platen increases.

Next, we analyze the behavior of two bodies in contact that can both deform by dislocation plasticity, as presented in Chapter 4. Given that the plastic behavior is unaffected by the contact conditions, contact is assumed frictionless. A size effect is found for two metal crystals in contact with different material properties, and unexpectedly, the effect is quantitatively the same. This is because a pure single metal crystal with a higher elastic modulus typically has, on average, a larger source strength. Larger stresses are hence required to induce plastic

deformation in the crystal.

It is also found that the response of two plastically deformable bodies in contact can be simplified to an equivalent contact problem where one body is rigid and the other can deform plastically. This is provided that the source strength in the equivalent problem is that of the softest material in the original problem, and that the source density is equal to the sum of the source densities contained in the two deformable crystals.

In Chapter 5 the shear behavior of sinusoidal asperities in contact with a platen pre-loaded with a constant normal force is examined. The only dissipative process is plasticity. The friction force, defined as the constant tangential force attained during shearing, is found independent of whether the platen is rigid, elastic, or even plastic. When the applied normal force is increased the friction force and the friction coefficient decrease. The local friction coefficient along the contact is highly non-uniform, and can be a few times larger than the average coefficient. The friction force and the friction coefficient are also found to be size dependent: smaller asperities have larger friction coefficients. This is attributed to a plasticity size effect in flattening.

6.2. DISCUSSION

FUNDAMENTAL understanding of plastic deformation on contact and friction gained from this work refines our thinking and approach in determining and analyzing the contact behavior of two crystals that can both plastically deform. We showed in Chapter 3 that a surface, initially smooth, becomes rough by formation of surface steps during loading. This is due to the discreteness of the dislocations and slip planes. Contact becomes patchy after loading, resulting in a contact pressure distribution characterized by high peaks.

Unfortunately there exist, up to date, no experiments that allow us to visualize how the steps left behind by escaped dislocations affect the contact areas at the (sub)-micron scale. It is a challenge to observe the influence of surface steps on the areas *in situ*, since steps are very small, in the order of nanometers. Visualization is also complicated by the fact that a surface is inherently rough [1–3]. Moreover, it is difficult to determine the size of contact at this length scale, since electrostatic interactions between atoms near the contact edges are significant and long ranged. However, we expect that in the near future experiments of this kind will become available, thanks to recent advancements in experimental techniques for visualizing contact *in situ* (see e.g. [2–5]).

Size effect observed at the (sub)-micrometer scales is attributed to source limitation (Chapter 3 and Chapter 4), which is well captured by the discrete dislocation plasticity method. Given that in reality a surface is composed of asperities

with sizes that can span over several scales, macroscale studies of rough surface contact should account for the fact that smaller (sub)-micrometer sized asperities have a different plastic behavior than larger asperities, so to more accurately predict the mechanical contact response of the surfaces.

Since the plastic properties of two crystals can be mapped into the plastic properties of one crystal in contact with a rigid body (Chapter 4), conclusions obtained from previous plasticity studies of contact with a rigid body apply to two crystals in contact with equivalent plastic properties and the same contact conditions.

Contact analysis of two crystals can be simplified to treat a single plastically deformable body in contact with a rigid body. The effect of the rigid body can also be mimicked by a set of boundary conditions at the contact, provided however, that the conditions are correctly prescribed. The rigid body effect will not be accurately captured, for instance, when we analyze a problem in which both bodies in contact are pre-loaded with a constant normal force. This is because the contact area and the normal displacement are unknown *a priori*, and a pressure distribution must be assumed at the interface. The distribution, as observed in the simulations, is non-uniform and it changes with loading. As a result the contact pressure will not be accurately described by boundary conditions. In this case both bodies have to be explicitly modeled.

Here, we demonstrate that when glide of dislocations in the material is the sole dissipation process the friction coefficient decreases with increasing applied normal force (Chapter 5). This has been similarly observed in friction experiments carried out on metals [6–8]. The friction coefficient also decreases to within the range of coefficient values reported by experiments for metals. Dissipation by plasticity is expected to be significant, and should not be excluded in the analysis of friction between metals in contact.

6.3. RESEARCH RECOMMENDATIONS

EQUIPPED now with the knowledge of how plasticity affects the mechanical behavior of bodies with sinusoidal surface in contact, the investigation can be further extended to predict the contact behavior of surfaces with a more elaborate description of roughness, i.e. a surface comprising asperities having different geometry. This will bring us a step closer to understanding the contact response between realistic rough surfaces. One promising way of describing surfaces is by considering self affinity of the roughness at different scales. This addresses the problem that the roughness parameters obtained from measurements, such as root mean square height and slope, are dependent on the resolution limit of the measuring instruments.

The contact model can be further modified to include frictional sliding between surfaces, by adding a kinetic energy term to the potential energy functional presented in Chapter 2. This term accounts for the rate of change of the tangential gap function g_t. The purpose would be to understand how dissipation by sliding at the contact, in addition to dissipation by plasticity in the material, would affect the response. For flattening we observe that the mechanical response is unaffected by the contact conditions. However, it is expected that the friction force is affected when frictional sliding occurs. The immediate challenge lies in determining the criteria for the onset of surface slip [9]. It is then necessary to understand the mechanisms precipitating slip at the contacts, e.g. relative motion between surfaces by dislocation glide or crack growth across the interface, which are candidates for further analysis.

If one is interested to predict realistically the mechanical behavior of two bodies deforming during contact, the model can be extended to include a third spatial dimension. In our study the dislocation line is straight and infinitely long. Dislocations in real solids have however, finite curvatures, and they can form complex three dimensional structures by entanglements and connections (see e.g. [10]). This will in turn affect the relaxation of the stresses in the body and hence the results compared with that obtained in our study. However, it is not obvious how, given the complexity of the dislocation interactions. Further analysis is therefore required.

REFERENCES

[1] F. P. Bowden and D. Tabor, *The friction and lubrication of solids*, Vol. 1 (Oxford: Claredon, 1950).

[2] K. N. Bachus, A. L. DeMarco, K. T. Judd, D. S. Horwitz, and D. S. Brodke, *Measuring contact area, force, and pressure for bioengineering applications: using Fuji Film and TekScan systems,* Med. Eng. Phys. **28**, 483 (2006).

[3] T. Suhina, B. Weber, C. E. Carpentier, K. Lorincz, P. Schall, D. Bonn, and A. M. Brouwer, *Fluorescence microscopy visualization of contacts between objects,* Angew. Chem. **127**, 3759 (2015).

[4] S. Rubinstein, G. Cohen, and J. Fineberg, *Visualizing stick–slip: experimental observations of processes governing the nucleation of frictional sliding,* J. Phys. D: Appl. Phys. **42**, 214016 (2009).

[5] D. J. Flannigan, S. T. Park, and A. H. Zewail, *Nanofriction visualized in space and time by 4D electron microscopy,* Int. Nano Lett. **10**, 4767 (2010).

[6] E. Rabinowicz, *Friction coefficients of noble metals over a range of loads,* Wear **159**, 89 (1992).

[7] I. Etsion and M. Amit, *The effect of small normal loads on the static friction coefficient for very smooth surfaces,* J. Tribol. T. ASME. **115**, 406 (1993).

[8] A. Ovcharenko, G. Halperin, and I. Etsion, *Experimental study of adhesive static friction in a spherical elastic-plastic contact,* J. Tribol. T. ASME. **130**, 021401 (2008).

[9] O. Ben-David, G. Cohen, and J. Fineberg, *The dynamics of the onset of frictional slip,* Science **330**, 211 (2010).

[10] D. M. Norfleet, D. M. Dimiduk, S. J. Polasik, M. D. Uchic, and M. J. Mills, *Dislocation structures and their relationship to strength in deformed nickel microcrystals,* Acta Mater. **56**, 2988 (2008).

ACKNOWLEDGEMENTS

Optimistic, passionate, uncertain, and thankful are words that summarize what I felt during the course of my doctoral research. Back then I contemplated doing my PhD overseas, since this means giving up the security and comfort offered by my home country, Singapore, i.e. my family, ample job opportunities, and a conducive research environment. Besides, as familiar as we are to the concept of a globalized society we live in today, adapting to another country and the culture usually takes years, and unequivocally the environment forms an intricate bond with our well being and our ability to perform. I must however confess, that this

A ship is safe in harbor, but that's not what ships are for.

William Shedd

has been one incredible journey that has no doubt played a huge role in shaping who I am now. With this thesis I close this chapter of my life, and I shall conclude by acknowledging the people who have been there for me and have made a positive influence in my life.

My special thanks goes out to my copromoter, dr. Lucia Nicola, for her guidance and encouragement throughout my PhD. Your experience in research has been a source of engaging discussions we had, and your critical eye for details has notched up the quality of my research work output. I am particularly thankful to you for taking up the role as my supervisor when I started with a new research topic, and for supporting my project partly with your 'VIDI' grant.

Progress depends upon the degree of sustained intensity in a given direction.

Roger McDonald, *The Message of a Master*

To my promoter prof. dr. Barend Thijsse, I appreciate your interest and effort in reviewing my thesis dissertation and propositions. Your advice and criticality have helped me when I was drafting my propositions, which proves to be challenging since a proposition is not a statement or question but an interesting and original comment, proposal, or opinion, and it should be opposable and defendable at the same time.

We, as doctoral researchers, are known devote most of our 'awake' time to our project. I was no exception, although I do remind myself not to make it the only purpose of going abroad to do my education. It would be unfortunate if I missed the 'rich' dutch culture, and embrace a lifestyle different from what I am used to. My appreciation goes out to the people I have encountered here, for which some have been a great source of inspiration for me.

To Maurice Boon and Jeroen Beijer, I enjoyed your company and the adventures we had! Together with David Zaccai you guys have greatly enlightened me (positively) with your way of life, e.g. the rules of engagement in cycling, and the frugal nature of the dutch people. A toast to our interesting conversations we had about cultures, travels and life experiences! Also to one of my tai chi mates Jeroen Heldens, your generosity and kindness have been a great influence.

One of the beautiful qualities of true friendship is to understand and to be understood.

Lucius Annaeus Seneca

My life in and outside the department would not be more enriched if not for these guys, the ever friendly, frivolous (perhaps occasionally) Casper Versteylen, energetic emphatic empath Ann-Sophie Farle, and physicist trained Robbert-Jan Dikken and his quip over our beings devoid of purpose. Many thanks to you guys for being a great source of inspiration, company and help!

Within the department I am grateful to Astrid Gubbels-Elzas, dr. Marcel Sluiter, Anke Kerlaan-Koene, dr. Murugaiyan Amirthalingam, dr. Marcel Hermans, Kees Kwakernaak, dr. Wim Sloof and prof. dr. Ian Richardson for their help and suggestions provided during my life as a PhD researcher. Not forgetting Julia Stikkelman, Alexandra Lucia Carabat, Myrthe Bosch, Shunsuke Yoshioka and Christian Klusmann, I have enjoyed our dinner outings and borrel activities. To my office mates, Mohsen Khajeh Salehani, dr. Nilgoon Irani, you have added more insanity to our cosy office room. Also to Prashanth Srinivasan, Social Group people (you know who you are), Erik Simons, dr. Amarante Bottger, dr. Dennis Braekmans, Hans Brouwer, Linda Boatemaa, Xi Zhang, Peter Klaver, Jan Steven van Dokkum, Syam Parayil Venugopalan, Lu Shen, and William Mao, our lunch/tea-break conversations are valued!

I would next like to acknowledge the following from my previous department who have contributed positively in my life. Specially to dr. Jodi Kooijman and dr. Antonio M.Recurero from the bicycle lab, prof. dr. Fred Van Keulen, dr. Matthijs Langelaar, dr. Hans Goosen, Marianne Stolker, Birgit Rademakers-Boot and Marli Guffens, I appreciate your assistance and suggestions offered when I was still in the department. Cheers also to our interesting coffee breaks, dr. Paul van der Valk, dr. Sven Voormeeren, Floris van Kempen, Evert Hooijkamp, Rob Eling, dr. Alexander Verbart, Rob Dedden, Marco Zocca and dr. Berkan Öztürk.

To the extensive list of others whom I have encountered here, especially during tai chi, swimming, gym, Red (Orange) Cross and WJD Madrid, you guys have also influenced my life in one way or another, and I extend my dedication to you.

Lastly, I would like to thank my family, who, although living thousands of miles apart, has always been there for me. I deeply appreciate your understanding and your support throughout these years.

CURRICULUM VITÆ

Kelvin NG WEI SIANG

07-12-1985	Born in Singapore.

EDUCATION

1998–2004	'O' and 'A' (Special) levels (Singapore-Cambridge) Northland Secondary School (1998–2002) Yishun Junior College (2003–2004)
2006–2010	Bachelor of Engineering with 1st Class Honors Aerospace Engineering Nanyang Technological University
2012–2016	Ph.D. Computational Solid Mechanics and Materials Science Department of Materials Science and Engineering Delft University of Technology *Thesis:* Modeling Contact between Plastically Deformable Crystals at the Micrometer Scale *Promotor:* Prof. dr. B. J. Thijsse

AWARDS

2010	Valedictorian
2010	Lew Kwan Yew Gold Medal
2010	Koh Boon Hwee Scholars Medal
2010	Defense Science Organization Gold Medal

LIST OF PUBLICATIONS

3. **K. Ng Wei Siang, and L. Nicola**, *Static Friction of Sinusoidal Asperities: A Discrete Dislocation Plasticity Analysis*, submitted to Acta Mater.

2. **K. Ng Wei Siang, and L. Nicola**, *Contact between Two Plastically Deformable Crystals: A Discrete Dislocation Dynamics Study*, submitted to Philos. Mag.

1. **K. Ng Wei Siang, and L. Nicola**, *Discrete Dislocation Plasticity Analysis of Contact between Deformable Bodies of Simple Geometries*, Model. Simul. Mater. Sci. **24**, 045008 (2016).

CONFERENCES

7. **K. Ng Wei Siang, and L. Nicola**, International Conference of Industrial Applied Mathematics (2015).

6. **K. Ng Wei Siang, and L. Nicola**, *Contact between Plastically Deformable Surfaces*, Physics@FOM Veldhoven (2015).

5. **K. Ng Wei Siang, and L. Nicola**, *Contact Analysis between Rough Surfaces using Discrete Dislocation Plasticity*, Gordon Tribology Conference (2014).

4. **K. Ng Wei Siang, and L. Nicola**, *Contact between an Elastic and a Plastically Deformable Surface*, Physics@FOM Veldhoven (2014).

3. **K. Ng Wei Siang, and L. Nicola**, *Discrete Dislocation Contact Model for Two Surfaces in Contact*, Material Research Society Conference (2013).

2. **K. Ng Wei Siang, and L. Nicola**, *Discrete Dislocation Plasticity Analysis of Contact between a Sinusoidal Metal Surface and a Flat Elastic Platen*, Physics@FOM Veldhoven (2013).

1. **K. Ng Wei Siang, G. van Zwieten, and M. A. Gutirrez**, *An Alternative Method for Simulation of 2D Discrete Dislocations*, European Congress on Computational Methods in Applied Science and Engineering Conference (2012).

WORKSHOPS

11. **K. Ng Wei Siang, and L. Nicola**, Materials Technology Day, Mauritshuis (2015)

10. **K. Ng Wei Siang, and L. Nicola**, Gordon Research Seminar, Bentley University, Waltham, MA (2014)

9. **K. Ng Wei Siang, and L. Nicola**, Schontal Symposium-Dislocation Based Plasticity, Kloster Schöntal (2014)

8. **K. Ng Wei Siang**, Mechanics in Micro-systems, Graduate School of Engineering Mechanics (2012)

7. **K. Ng Wei Siang**, Advanced Topics in Solid Mechanics, Graduate School of Engineering Mechanics (2012)

6. **K. Ng Wei Siang**, Upscaling Techniques and Homogenization, Johannes Martinus Burgers Centrum (2011)

5. **K. Ng Wei Siang**, Reliability and Stability in Statics and Dynamics, Graduate School of Engineering Mechanics (2011)

4. **K. Ng Wei Siang**, Optimization and Parameter Identification, Graduate School of Engineering Mechanics (2011)

3. **K. Ng Wei Siang**, Experimental Engineering Mechanics, Graduate School of Engineering Mechanics (2010)

2. **K. Ng Wei Siang**, Multi-scale and Micro-mechanics, Graduate School of Engineering Mechanics (2010)

1. **K. Ng Wei Siang**, Mechanics of Large Deformations, Graduate School of Engineering Mechanics (2010)